

Review

# Porous Carbon for CO<sub>2</sub> Capture Technology: Unveiling Fundamentals and Innovations

Gazi A. K. M. Rafiqul Bari \*  and Jae-Ho Jeong \*

School of Mechanical Smart and Industrial Engineering, Gachon University, 1342 Seongnam-daero, Sujeong-gu, Seongnam-si 13120, Gyeonggi-do, Republic of Korea

\* Correspondence: grafiquibari@gachon.ac.kr (G.A.K.M.R.B.); jaeho.jeong@gachon.ac.kr (J.-H.J.);  
Tel.: +82-42-750-5654 (J.-H.J.)

**Abstract:** Porous carbon is an emerging material for the capture of CO<sub>2</sub> from point sources of emissions due to its high structural, mechanical, and chemical stability, along with reusability advantages. Currently, research efforts are mainly focused on high- or medium-pressure adsorption, rather than low-pressure or DAC (direct air capture) conditions. Highly porous and functionalized carbon, containing heteroatoms (N, O, etc.), is synthesized using different activation synthesis routes, such as hard template, soft template, and chemical activation, to achieve high CO<sub>2</sub> capture efficiency at various temperatures and pressure ranges. Fundamental pore formation mechanisms with different activation routes have been evaluated and explored. Higher porosity alone can be ineffective without the presence of proper saturated diffusion pathways for CO<sub>2</sub> transfer. Therefore, it is imperative to emphasize more rational multi-hierarchical macro-/meso-/micro-/super-/ultra-pore design strategies to achieve a higher utilization efficiency of these pores. Moreover, the present research primarily focuses on powder-based hierarchical porous carbon materials, which may reduce the efficiency of the capture performance when shaping the powder into pellets or fixed-bed shapes for applications considered. Therefore, it is imperative to develop a synthesis strategy for pelletized porous carbon and to explore its mechanistic synthesis route and potential for CO<sub>2</sub> capture.

**Keywords:** porous carbon; micropores; ultra-micropores; biomass; CO<sub>2</sub> capture; surface functionalized; hierarchical structure; super-micropores; chemical activation; template strategy



**Citation:** Bari, G.A.K.M.R.; Jeong, J.-H. Porous Carbon for CO<sub>2</sub> Capture Technology: Unveiling Fundamentals and Innovations. *Surfaces* **2023**, *6*, 316–340. <https://doi.org/10.3390/surfaces6030023>

Academic Editor: Pasquale Fernando Fulvio

Received: 28 July 2023

Revised: 27 August 2023

Accepted: 15 September 2023

Published: 18 September 2023



**Copyright:** © 2023 by the authors. Licensee MDPI, Basel, Switzerland. This article is an open access article distributed under the terms and conditions of the Creative Commons Attribution (CC BY) license (<https://creativecommons.org/licenses/by/4.0/>).

## 1. Introduction

The industrialization and urbanization of humans have resulted in a significant increase in CO<sub>2</sub> emissions, estimated to be over 36 billion tons at present [1]. As a consequence, the current CO<sub>2</sub> concentration levels in the environment have reached ~420 ppm, compared to ~280 ppm during preindustrial times (Figure 1) [2,3]. This increase is certain to cause hugely detrimental effects on human life through climate change. It requires immediate efforts to adopt a net-zero strategy to mitigate CO<sub>2</sub> effects by efficiently capturing CO<sub>2</sub> from point sources (such as oil refineries, heavy industries, cement, fossil fuel power plants, and industrial process plants) or through direct air capture (DAC) [4–6].

Over the years, CO<sub>2</sub> capture or separation from flue gases has seen the development of the chemical absorption technique utilizing liquid alkanolamine solution process (scrubbing) on an industrial scale [7,8]. The liquid amine absorption technique has reached an industrial state-level advancement with considerable CO<sub>2</sub> capture capacity (1.5 mmol g<sup>-1</sup>) and absorption rate (0.05–0.18 mol m<sup>-2</sup> s<sup>-1</sup>) at a 4–25 vol.% concentration level [7,9,10]. Primary and secondary amines form carbamate with comparatively higher reaction kinetics with CO<sub>2</sub>, requiring high enthalpy absorption reactions of 80–90 and 70–75 kJ mol<sup>-1</sup> CO<sub>2</sub>, respectively. In the case of tertiary amines, they form bicarbonate with CO<sub>2</sub> with sluggish reaction kinetics, requiring 40–55 kJ mol<sup>-1</sup> CO<sub>2</sub> absorption enthalpy through a base-catalyzed hydration mechanism [11–13].

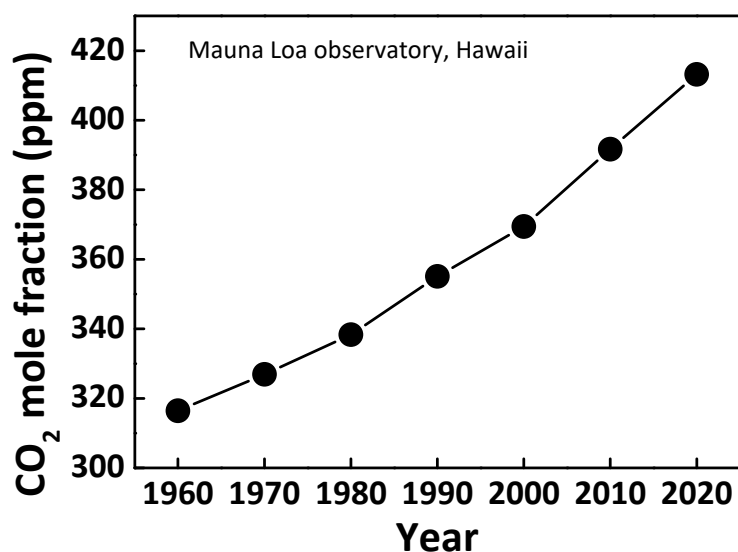


**Figure 1.** CO<sub>2</sub> concentration monitoring by decade (1960~present) by ESRL's (Earth System Research Laboratories) Global Monitoring Laboratory (GML) at Mauna Loa observatory in Hawaii.

Consequently, solvent regeneration (stripping) requires a huge amount of energy (3–5 GJ t<sup>-1</sup> CO<sub>2</sub> captured), leading to large-scale industrial energy consumption and adding to the 70% additional cost, which is the main obstacle. However, the acceptable value for industrial application is 0.4–0.7 GJ t<sup>-1</sup> CO<sub>2</sub> [14–16]. Furthermore, the liquid amine absorption process faces other hurdles, such as liquid amine degradation due to high heating, solvent loss, equipment corrosion of reactors (steel/carbon), production of carcinogenic toxic products (nitramines, nitrosamines), and the utilization of large amounts of NaOH or KOH to restore CO<sub>2</sub> absorption capacity of amines, resulting in a secondary pollutant to alkaline wastewater [17,18].

To address the drawbacks of the liquid amine absorption process mentioned above, the physical adsorption technique has become a focal point. CO<sub>2</sub> physisorption on porous sorbent surfaces provides lower adsorption enthalpy (15–50 kJ mol<sup>-1</sup>) [19,20]. Consequently, the regeneration of CO<sub>2</sub> gas molecules requires lower energy consumption and provides a completely clean surface for reusability. Solid adsorbents, such as MOFs (metal–organic frameworks), COFs (covalent–organic frameworks), zeolites, and carbon, offer alternative options for CO<sub>2</sub> sorption from point sources, countering the drawbacks of the aqueous liquid amine absorption technique (84 kJ mol<sup>-1</sup>, USD 45–80 per ton of CO<sub>2</sub> capture) [21]. Compared to the liquid amine absorption technique, solid adsorption offers lower heat of adsorption (MOF: 50 kJ mol<sup>-1</sup>, COF: 30–50 kJ mol<sup>-1</sup>, zeolites: 30–50 kJ mol<sup>-1</sup>, carbon: 10–35 kJ mol<sup>-1</sup>) [11,20,22]. Comparing the approximate capital costs/operation and maintenance expenses, including abandonment costs, for CO<sub>2</sub> capture using polymeric membranes, chemical absorption, and physical absorption reveals values of USD 640/290, 839/365, and 590/271 million, respectively [23–25]. Depending on the specific characteristics and properties (surface area, pore volume, porosity, interconnected pore structure, surface functionality, etc.) of the solid adsorbent, an efficient level of capture and separation from flue gas can be achieved after post-combustion capture [26,27].

One of the technical criteria for solid adsorbent capture is the consideration of capture under dry conditions to ensure a reasonable capture efficiency. However, most of the post-combustion flue gas remains wet (5–7 vol.% water) at 40–80 °C, necessitating an energy-intensive drying process to remove moisture from the multi-component flue gas flow [27,28]. Ultimately, removing moisture from the gas flow or drying it backfires in terms of technical feasibility on an industrial scale. Additionally, wet condition CO<sub>2</sub> capture significantly reduces the efficiency of MOF-, COF-, and zeolite-based solid adsorbents due to lower hydrothermal stability [27,29]. In comparison, carbon-based materials exhibit

comparable stability under moisture and thermal conditions due to the structural and mechanical rigidity of the carbon structure.

Among the solid adsorbents, carbon-based adsorbents are considered promising candidates for CO<sub>2</sub> capture technology due to their abundant sources, low cost, and scalable preparation process [30]. Additionally, carbon-based materials are known for their good thermal and chemical stability, low energy regeneration, and ability to maintain adsorption performance even under high moisture conditions [31,32]. They also offer the benefit of tunable opportunities for textural properties and surface functionalization [33].

## 2. Carbon as a Promising Candidate for CO<sub>2</sub> Capture Technology

Carbon is considered a promising candidate for CO<sub>2</sub> capture technology due to its capacity to offer a clean surface for reutilization, along with its thermal, mechanical, chemical, and moisture stability [34]. Its simple preparation strategy and low cost make it suitable for industrial applications [35].

A large variety of precursor sources, primarily biomass-based, such as rice husk, coconut shells, shrimp shells, sawdust, microalgae, carrot, olive stones, almond shells, kiwi peel, sugar beet pulp, palm stone saccharides, and glucose, are available [36]. Different activation strategies, including chemical methods (using urea, KOH, NaOH, ZnCl<sub>2</sub>, H<sub>3</sub>PO<sub>4</sub>, K<sub>2</sub>CO<sub>3</sub>, H<sub>2</sub>SO<sub>4</sub>, HNO<sub>3</sub>, HCl, H<sub>3</sub>PO<sub>4</sub>/KOH, NaOH, ZnCl<sub>2</sub>, CaCl<sub>2</sub>, K<sub>2</sub>CO<sub>3</sub>/H<sub>2</sub>O<sub>2</sub>, and KMnO<sub>4</sub>), physical methods (using oxidizing gases like O<sub>2</sub>, CO<sub>2</sub>, steam, air, and NH<sub>3</sub>), and both hard (using molten salt, eutectic salt, MOF, silica, zeolite) and soft (using organic precursors like melamine and cyanuric acid) approaches, can be employed to tailor the pore size and shape of the carbon structure [21,37].

Various templating methods, including gas templates, hard templates, soft templates, and chemical activation, are employed to design ultra-super-micropores for low-pressure CO<sub>2</sub> capture and macro-mesopores for high-pressure CO<sub>2</sub> capture [1]. Heteroatom doping on carbon and surface modification induces hetero-surface functionalized groups on the carbon structure to control surface chemistry [38,39]. CO<sub>2</sub> molecules, being of acidic nature and possessing a quadrupole moment, have a competitive advantage over other gases for surface sorption due to the surface chemistry. Essentially, weak van der Waals forces induce the physisorption of CO<sub>2</sub> molecules on the surface, which can be intensified by functional groups, such as acid-base interactions, H-bonds, or electrostatic interactions. As a result, this leads to a higher adsorption capacity for CO<sub>2</sub> compared to other gas mixtures, making it more selective towards CO<sub>2</sub> molecules [40,41].

During carbonization, a higher degree of aromaticity imparts a hydrophobic nature to carbon, allowing it to function effectively under hydrated conditions [42]. However, while heteroatom doping reduces polyaromatic condensation and reduce mechanical and chemical stability, it is essential to seek a rational design strategy for synthesizing carbon materials [43,44].

### 2.1. Carbon Products Preparation Mechanism

A carbon synthesis technique utilizes various technical processes such as pyrolysis (400–1100 °C), sol-gel, and hydrothermal processes [45]. Hydrothermal technology utilizes water as a medium in a closed reactor vessel to undergo processes such as hydrolysis, dehydration, decarboxylation, concentration polymerization, and aromatization [46]. It aligns with the principles of thermochemical conversion, making it a sustainable and green process similar to the natural formation of carbon. Hydrothermal methods offer the opportunity to produce various initial intermediate products that can later be combined with the general pyrolysis process, enabling the diversification of morphological and structural properties [47,48]. Pyrolysis is a thermochemical conversion process where materials decompose into solid (char), liquid (oil), and gas (syngas) as the temperature increases. The properties of pyrolysis products depend on various factors, including temperature, residence time, heating rate, and whether fast or slow pyrolysis is employed. In the con-

ventional pyrolysis process, a furnace's heating wall transfers heat to the material's surface, resulting in a higher yield of char compared to microwave pyrolysis [49,50].

Fundamental carbon formation mechanisms bear the dehydration, intramolecular condensation, decarboxylation, and polymerization for oxygen-containing functional groups in the different temperature ranges (Figure 2) [1,51]. Various techniques or different sources are utilized in the formation of different intermediate products to provide the different characteristic carbon products. Initially, various sources or technical processes yield diverse intermediate products through dehydration, intramolecular condensation, or initial polymerization, resulting in an intermediate structural framework [52]. With increasing temperature, aromatic polycondensation steps occur, generating multiple gas components like  $\text{NH}_3$ ,  $\text{CH}_4$ ,  $\text{CO}$ ,  $\text{CO}_2$ ,  $\text{H}_2$ , water vapor, or structural degradation, which create structural, internal, and surface pores. Additionally, pressure modifies or influences the shape of the carbon [53,54].

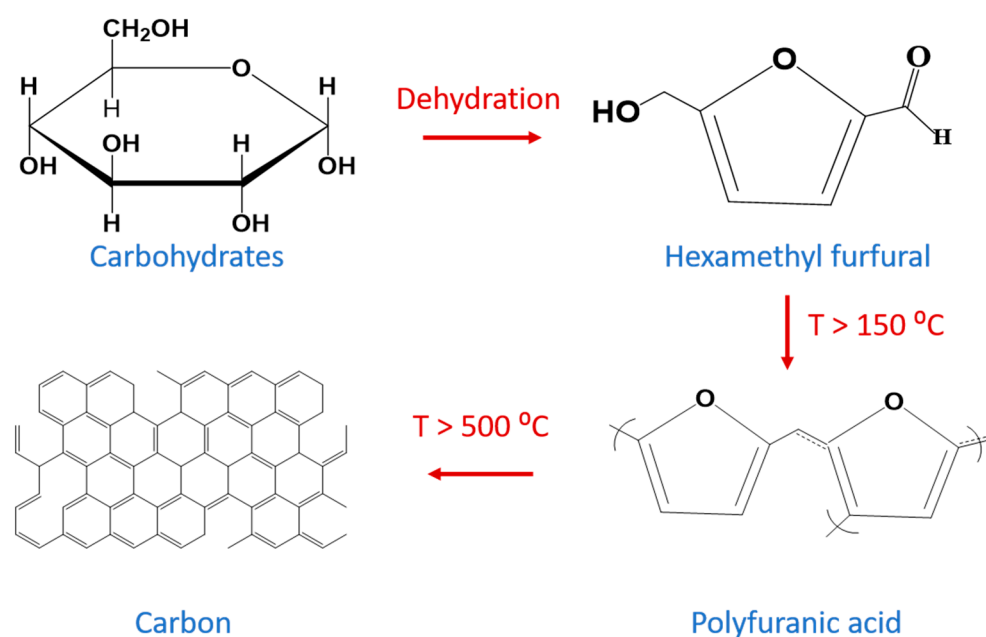


**Figure 2.** A schematic representation elucidating the mechanisms of carbon formation.

## 2.2. Factors Influencing $\text{CO}_2$ Adsorption on the Carbon Surface

The number of  $\text{CO}_2$  molecules adsorbed on the surface depends on several factors, including surface area, cumulative pore volume, pore sizes, pore interconnectivity, pore shape, and surface chemistry [55]. The low-pressure or high-pressure capture efficiency depends on the textural properties of the adsorbents. It is suggested that low-pressure conditions are overwhelmed by ultra-micropores (0.35–0.70 nm) to super-micropores (0.70–0.90 nm). At high-pressure conditions, pores size greater than micropores is more favorable [56,57]. Also, it is important to consider the competition among the different gases ( $\text{CO}_2$ ,  $\text{N}_2$ ,  $\text{NO}_x$ ,  $\text{SO}_2$ ,  $\text{H}_2\text{O}$  vapor, etc.) to be separated or captured at a point source [58]. The kinetic diameter of  $\text{CO}_2$  (0.33 nm) is smaller than the kinetic diameters of nitrogen (0.36 nm) and oxygen (0.34 nm);  $\text{CO}_2$  adsorption favors the smaller than micro-size pores (<2 nm), while  $\text{N}_2$  adsorption is more favorable at mesoporous volumes (>2 nm) [59]. Surface chemistry of the adsorbents influences the  $\text{CO}_2$  sorption amounts, selectivity, dynamic kinetics due to  $\text{CO}_2$  molecule polarizability, and quadrupole nature. A  $\text{CO}_2$  molecule has higher polarizability ( $26.3 \times 10^{-25} \text{ cm}^3$ ) and quadrupole moment ( $13.4 \times 10^{-40} \text{ C m}^2$ ) in comparison to a  $\text{N}_2$  molecule of  $17.6 \times 10^{-25} \text{ cm}^3$  and  $4.7 \times 10^{-40} \text{ C m}^2$  [10,20,26].

$\text{CO}_2$  physisorption on a carbon surface occurs due to the weak van der Waals force. Heteroatoms or heteroatom-containing functional groups influence the  $\text{CO}_2$  adsorption on the surface of carbon, leading to more adsorption potential, depending on the types of in-

teractions (H-bond, electrostatic interaction, Lewis acid–base interaction) (Figure 3) [60–62]. There is still an ongoing debate about which types of interactions mainly occur or which forces are important in the CO<sub>2</sub> physisorption on the carbon surface. It can be assumed that higher polarizability and quadrupole moment of CO<sub>2</sub> molecules are more favorable for CO<sub>2</sub> molecules to separate from the other gases (N<sub>2</sub>, O<sub>2</sub>, H<sub>2</sub>, CH<sub>4</sub>, etc.) [63].

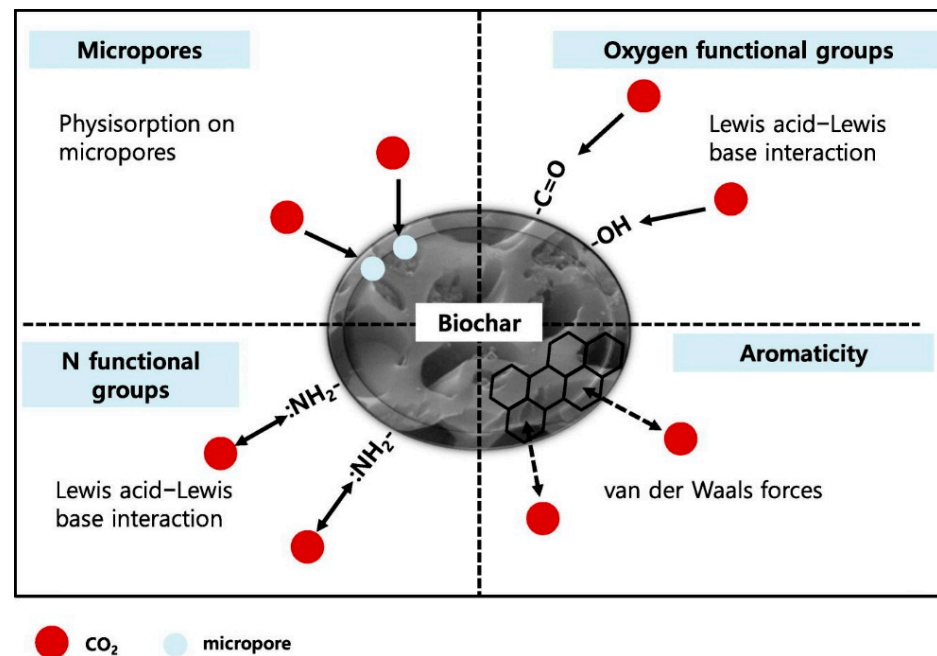


**Figure 3.** Graphical illustration that shows the CO<sub>2</sub> capture mechanisms on the carbon surface [64]. Adapted with permission from ref., copyright (2020) Elsevier Ltd.

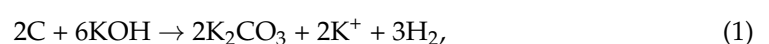
### 3. Strategies for Modifying Carbon Structures

A three-dimensional interconnected porous carbon synthesis strategy has been developed over the years to enhance the surface area, porosity, and gas diffusion rate of the components [37]. Various activation techniques for the carbon structure have been explored, including chemical activation, soft and hard template methods, and in situ metal ion activation strategies. The basic synthesis strategy, challenges, and minute factors that influence the structure of carbon are discussed in the following section.

#### 3.1. Chemical Activation

To produce highly porous and efficient carbon products, chemical activation of the carbon during carbonization has shown a potential utilization technique [65]. In the process, carbon precursors or carbon sources are simply mixed with an activating agent, and carbonization proceeds through different temperatures (350–800 °C) to achieve a porous carbon. Different acidic (e.g., HCl, FeCl<sub>3</sub>, ZnCl<sub>2</sub>, H<sub>3</sub>PO<sub>4</sub>, H<sub>2</sub>SO<sub>4</sub>, and HNO<sub>3</sub>), alkaline (e.g., KOH, NaOH, CaCO<sub>3</sub> and K<sub>2</sub>CO<sub>3</sub>), or oxidant substances (e.g., H<sub>2</sub>O<sub>2</sub>, and KMnO<sub>4</sub>) have previously been utilized as activating agents to activate the carbon during carbonization [66–68]. Utilizing such an activating agent provides a very effective way to reduce the carbonization temperature and induce porosity or shape modification during the formation process. However, it cannot omit the extra step of removing the corrosive chemical from the structure using water.

Different groups have tried to determine the activation mechanism, nearly in complete agreement. Most commonly, KOH was used as the chemical activation agent, being a strong base [65,69]. Most groups predict the carbonization reaction as Equation (1) [70]:



Afterward, some groups have shown that volatile groups from the precursor (CO, CO<sub>2</sub>, and H<sub>2</sub>O), upon heating, react with KOH and form K<sub>2</sub>CO<sub>3</sub>:



The metallic potassium (K), resulting from the reaction of the K<sub>2</sub>CO<sub>3</sub> with the carbon species, as well as its spatial positioning or penetration into the internal structure of carbon, promotes porosity. This internal porosity, upon removal during the washing step, provides the internal pore network:



A proper ratio of precursors to activating agents influences the textural, mechanical, and structural properties of the carbon products. An optimally high ratio of the activating agent (approximately 4) enhances the porosity of the carbon by intercalating its structure and resulting in expansion of the pores. However, with a higher ratio (>6), the excessive enhancement breaks the pore walls and reduces the overall porosity. A carbon nanosphere was hydrothermally prepared from glucose [71]. This process controlled the spherical shape of the precursor. Subsequent heat treatment and activation using a KOH solution were employed to introduce finely tuned ultra-micropores into the structure (Figure 4).

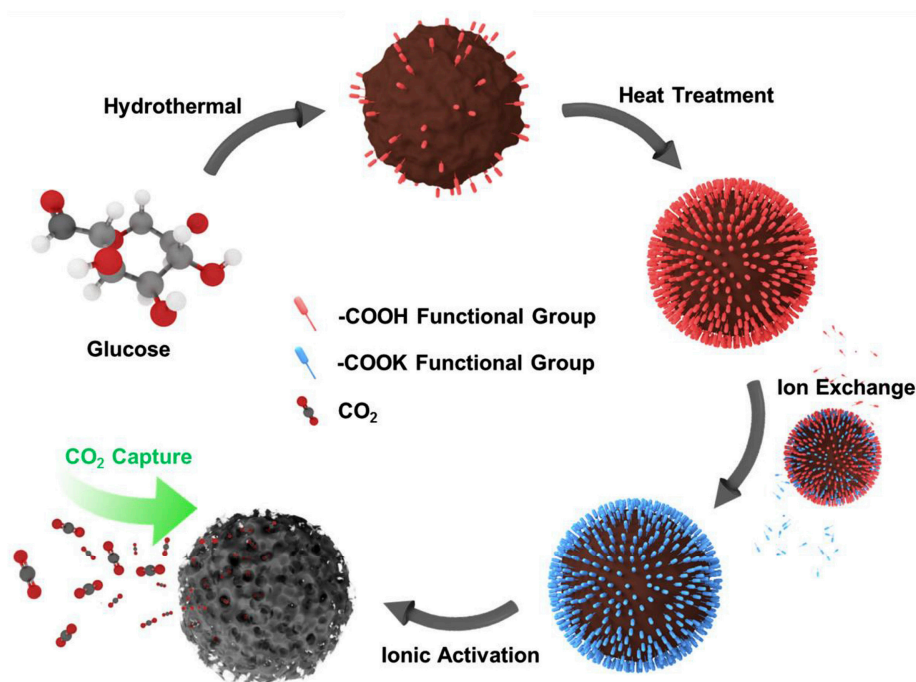


**Figure 4.** Synthesis strategy of ultra-microporous carbon nanosphere [71]. Adapted with permission from ref., copyright (2020) Elsevier Ltd.

### 3.2. Physical Activation

Physical activation is environmentally friendly, cheaper, simpler and requires no chemical agent. The gas template controls the textural properties [72,73]. During pyrolysis (300–1100 °C), degradation products generate different kinds of gas, such as CO<sub>2</sub>, CO, CH<sub>4</sub>, NO, H<sub>2</sub>O, and NH<sub>3</sub>, depending on the precursor's source [37]. Sometimes, external sources of media like CO<sub>2</sub>, NH<sub>3</sub>, steam, He, Ar, air, or a mixture of gases (binary mixture) are utilized to activate the carbon surface (Figure 5) [74–76]. Several efforts have been made to increase the pore volume and surface area by utilizing external steam during pyrolysis [77]. Steam, along with the pyrolysis temperature, interacts with carbon to produce C(O) and H<sub>2</sub>, which are sources of various activated gases such as CO, CO<sub>2</sub>, and CH<sub>4</sub>. Consequently, this process promotes the formation of new pores and the expansion

of pore sizes (Figure 5) [64,78]. The steam activation mechanism of the carbon surface is described in the following reactions [36,79]:

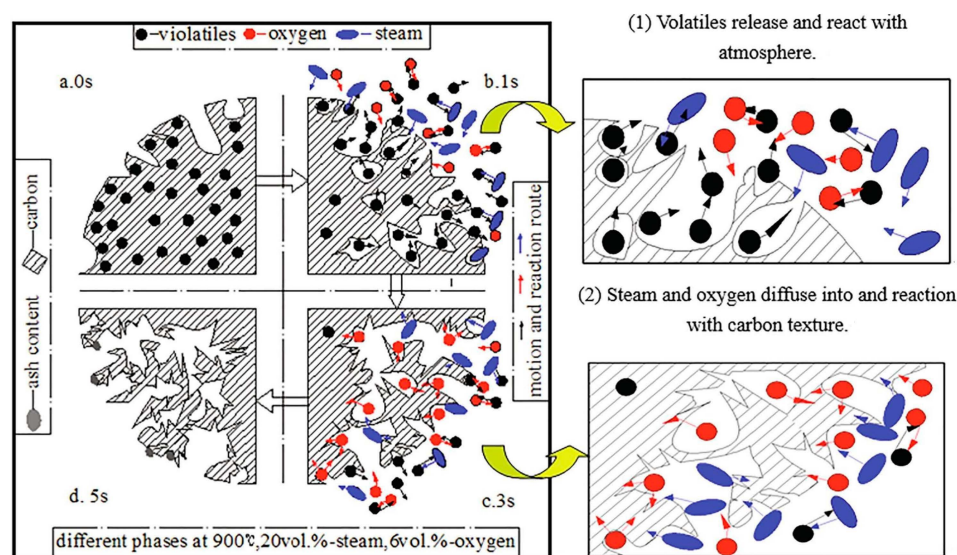


**Figure 5.** Schematic diagram showing the mechanisms of pore formation within the carbon structure during the physical activation process; (a–d) activation reaction time: 0, 1, 3, and 5 s, consecutively [78]. Adapted with permission from ref., copyright (2019) Elsevier Ltd.

Jung-Heo showed that steam activation of carbon from cellulose fiber expanded the existing ultra-micropores and produced additional ultra-micropores (Figure 6) [80]. The graphitic structure shattered due to the activation process, resulting in the size of the pores being larger than 2 nm. The activation process increased the specific surface area and pore volume to  $1018 \text{ m}^2 \text{ g}^{-1}$  and  $0.43 \text{ cm}^3 \text{ g}^{-1}$  from  $452 \text{ m}^2 \text{ g}^{-1}$  and  $0.199 \text{ cm}^3 \text{ g}^{-1}$ , respectively. Consequently, the  $\text{CO}_2$  capture performance reached  $4.41 \text{ mmol g}^{-1}$  at  $0 \text{ }^\circ\text{C}$ , 1 bar ( $1.21 \text{ mmol g}^{-1}$  at  $25 \text{ }^\circ\text{C}$ , 15%  $\text{CO}_2$ ) compared to without activation, which was  $3.18 \text{ mmol g}^{-1}$  at  $0 \text{ }^\circ\text{C}$ , 1 bar [80].

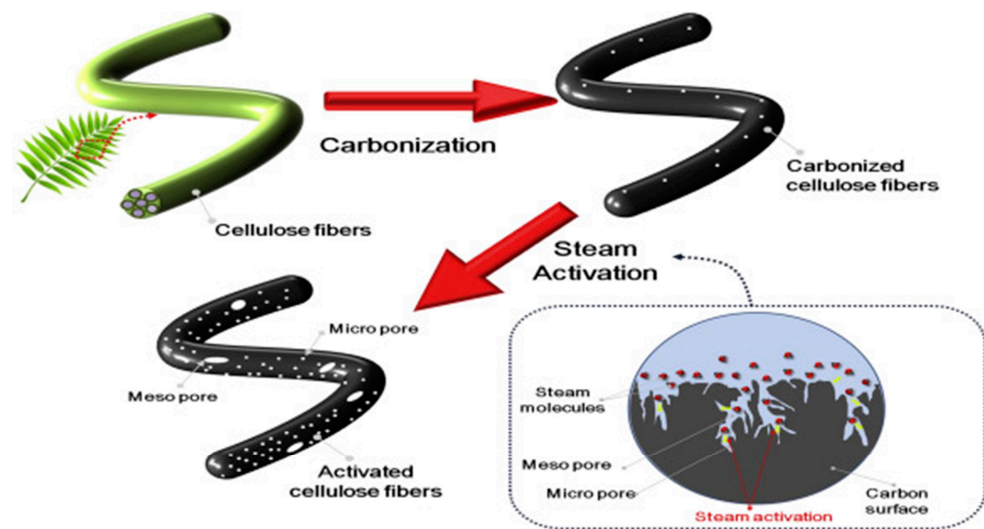
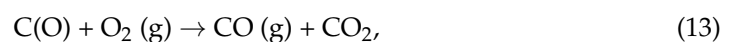
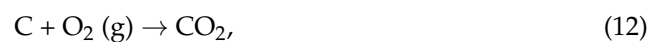


**Figure 6.** A schematic show of carbon surface activation by steam [80]. Adapted with permission from ref., copyright (2015) Elsevier Ltd.

Air activation is one of the efficient ways to simultaneously produce micropores and mesopores on the carbon surface while inducing O-containing functional groups such as C=O, C-O, -OH, and -COOH [81,82]. It is important to choose the activation time carefully. Initially, micropore formation on the carbon surface occurs predominantly, and, over time, it leads to an increase in mesopores due to the destruction of micropores [81,83]. The air activation mechanism of the carbon surface is described in the following reactions [84]:



In comparison to chemical activation, physical activation has less control over porosity development than chemical activation. The flow rate of  $\text{N}_2$  or other gases influences the textural properties of the carbonized products ( $10\text{--}200 \text{ mL min}^{-1}$ ). During the carbonization process, the gas template of the degradation products provides the basic porosity and shapes of the carbonized products [85]. The faster or slower removal of the gas template depends on the gas flow rate of the carbonization medium. The effects of the flow rate on textural properties and shapes need to be explored. Additionally, the activation time ( $0.5\text{--}72 \text{ h}$ ) plays a crucial role in determining the textural properties, as higher activation time and degree promote higher porosity in the structure. At the same time, the porosity range differs based on the activation time or temperature range of carbonization. Smaller pores (ultra-to-micropores, ultra-pores:  $0.35\text{--}0.70 \text{ nm}$ , super-micropores:  $0.70\text{--}0.90 \text{ nm}$ , micropores:  $0.90\text{--}2 \text{ nm}$ ) tend to shift to the range of higher pores with increasing temperature due to pore wall breakages that induce the conversion of super-micropores to mesopores [34,85].

### 3.3. Metal Ion Activation

The chemical and physical activation strategies are highly efficient for microporous carbon synthesis. Pores smaller than  $1 \text{ nm}$  (ultra-to-super-micropores) are particularly effective for low pressure  $\text{CO}_2$  uptake. Several research efforts have focused on the single-ion activation route to produce carbon with ultra-micropores in the structure [86]. In this process, monodispersed alkali metal ions ( $\text{Li}^+$ ,  $\text{K}^+$ ,  $\text{Na}^+$ ,  $\text{Rb}^+$ ,  $\text{Cs}^+$ ) are introduced into the carbon precursors of phenolic resin through a reaction between alkali hydroxide and the

acidic groups of the resin during the solution process [87]. Monodispersed metal ions induce ultra-micropores in the carbon structure and provide the opportunity to tune pore sizes at the angstrom or sub-angstrom level (0.6–0.76 nm), depending on their individual activation strength and metal ionic size. The technique of metal ion activation has made significant progress through the in situ homogeneous activation process. In this method, metal salts are combined with organic precursors, such as alkali metal salts of carboxylic phenolic resin, through a hydrothermal process to produce xerogel. Under a temperature of 400 °C, these compounds undergo decomposition, resulting in the creation of metal carbonate ( $M_2CO_3$ ), accompanied by the release of water vapor and  $CO_2$  gas, which act as templates. Moreover, the subsequent thermal decomposition of the metal carbonate ( $M_2CO_3$ ) facilitates the generation of metal oxide ( $M_2O$ ) through a redox reaction between the metal carbonate ( $M_2CO_3$ ) and carbon. This reaction is depicted by the equation  $M_2CO_3 + C \rightarrow M_2O + 2CO$ .

Furthermore, the metal oxide ( $M_2O$ ) significantly etches the carbon framework through a vigorous redox interaction between the metal oxide and the carbon framework. This is illustrated by the equation  $M_2O + C \rightarrow 2M + CO$ . As a result, the produced metallic component intercalates the crystalline graphitic lattice of the carbon. Consequently, this process leads to the expansion of the interlayer spacing within the lattice, thereby stabilizing the carbon structure. Subsequent to the washing process, in which the metallic portion is removed by water, the structure no longer reverts to its previous nonporous state. Instead, it retains the expanded lattice configuration, resulting in nanopores smaller than 1 nm. The precise size of these pores (spacing) can be finely tuned based on the dimensions of the metal ion, allowing for adjustment from  $Li^+$  to  $Cs^+$ . Zhou et al. produced N-doped, uniformly ultra-microporous carbon material of approximately 0.5 nm using a metal activation process on  $K^+$ -exchanged meta-aminophenol–formaldehyde resin [86]. This process led to a notable  $CO_2$  capture performance of 1.67 mmol  $g^{-1}$  under low pressure (0.15 bar, 25 °C).

### 3.4. Hard Template Activation

A hard template is utilized to associate with gaseous and solid carbon structures during high-temperature pyrolysis by duplicating or molecular printing on the surface of the template structure. The carbon can maintain its microstructure during the activation treatment process. Hard templates such as zeolites (zeolite x/y), porous metals (Zn–Co, Cu–Ni, Ni–Mn, etc.), metal powder (Ni/Cu powder), metal foam (Ni, Cu, Fe, etc.), silica (silica sphere, SBA-15, MCM-48), and MOFs (MOF-5, ZIF-8) have been explored to produce interconnected porous carbon structures [88,89]. Hard templates can provide effective and stable effects under confined conditions in spaces. In general, zeolites (0.1–10 nm), MOFs (0.1–50 nm), silica (10–1000 nm), salts (1 nm–10  $\mu m$ ), porous metals (100 nm–10  $\mu m$ ), metal powder (100 nm–1  $\mu m$ ), and metal foam (1  $\mu m$ –10  $\mu m$ ) are utilized to infuse various ranges of porosity into the carbon structure [89]. Recently, Joseph et al. successfully synthesized interconnected hierarchical carbon by utilizing Coca-Cola, a soft drink, combined with the hard template KIT-6 (mesoporous silica nanoparticles) and activating the carbon using  $ZnCl_2$  [90]. This method resulted in an impressively high specific surface area of 2003  $m^2 g^{-1}$ . In this process, the hard template acts as the source of the mesoporous structure, while  $ZnCl_2$  plays a pivotal role in enhancing micropores within the carbon structure and reducing the number of mesopores. However, an excessive use of the activation agent  $ZnCl_2$  can potentially lead to damage in both mesopore and micropore structures (Figure 7).

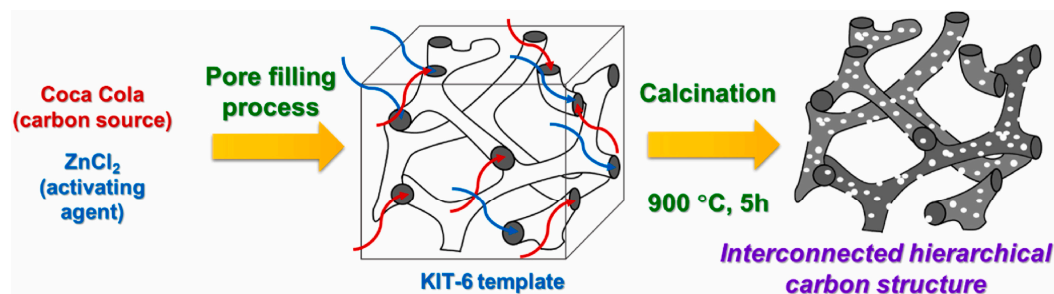


**Figure 7.** Diagram illustrating the synthesis process of interconnected hierarchical carbon using the KIT-6 hard template and  $\text{ZnCl}_2$  activation. [90]. Adapted with permission from ref., copyright (2023) Elsevier Ltd.

A molten salt, or a eutectic mixture of salts such as  $\text{LiBr}/\text{KBr}$  (348 °C),  $\text{LiI}/\text{KI}$  (275 °C),  $\text{LiCl}/\text{KCl}$  (353 °C), is utilized as a high-temperature solvent to synthesize porous carbon (Figure 8) [52,91–93]. In the synthesis process, the solvent intermediate products are carbonized under diluted conditions, resembling water under hydrothermal conditions, providing the opportunity for the formation of structured carbon [94]. Carbohydrate polymerization in the presence of strongly interacting metal ionic species creates nanopores in the carbon material, and the pore size can be tuned depending on the ionic species or the precursor-to-salt ratio. A proper choice of cation and counter anion controls the pore size. Additionally, the miscibility in the reaction medium with intermediate products, depending on their polarizability, influences the textural properties [95].

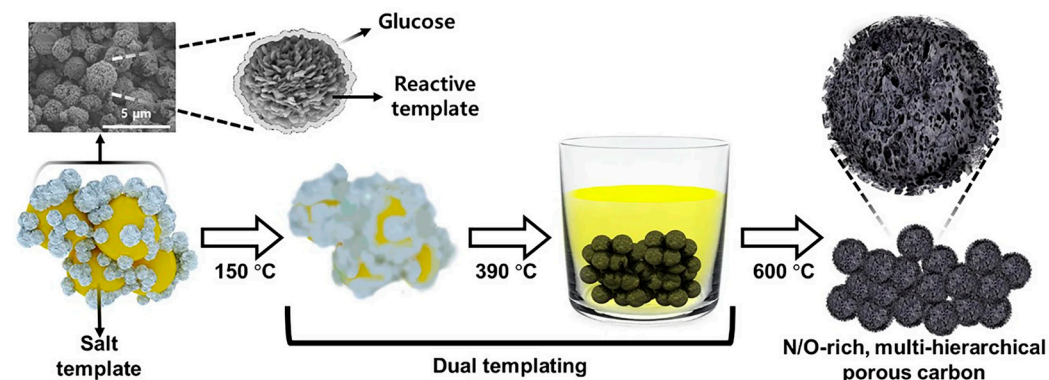


**Figure 8.** Hierarchical porous carbon synthesis from glucose utilizing  $\text{LiBr}/\text{KBr}$  molten salt and an organic reactive template of melamine–cyanuric acid complex [1]. Adapted with permission from ref., copyright (2023) Springer Nature.

In situ hard salt templates of  $\text{NaCl}$ ,  $\text{ZnCl}_2$ ,  $\text{Na}_2\text{CO}_3$ , and  $\text{CaCO}_3$  are utilized to enable large-scale production of carbon from glucose, sucrose, and biomass. This is due to their cheap and simple removal process through water washing steps. The silica and zeolite templates require  $\text{HF}$  or  $\text{NaOH}$ , while metal powder, porous metal, metal foam, and MOFs need an acidic solution for removal after shaping the carbon structure. Such types of aggressive removal steps sometimes damage the objective pores' structure to some extent [89,96].

Overall, hard template carbon offers greater mechanical stability and robustness when compared to reactive or soft template synthesis carbon. This type of carbon displays elevated surface area and structural integrity. Moreover, it enables the production of various ordered structures, including thin-walled carbon layers, sieving-specific pore sizes, ordered mesoporous carbon, and close-packed ordered hexagonal or cubic mesoporous carbon. It also leads to carbon with bimodal porosity [97,98]. Nonetheless, the utilization of hard-templated carbon comes with notable drawbacks. A significant challenge involves

the necessity of eliminating the hard template from the carbon through etching, achieved by an aggressive acid removal process like, when using a silica template, washing with HF or HCl. This extra step consumes time and resources. Additionally, hard-templated carbon is constrained in terms of pore size range, which becomes critical when aiming for a multi-hierarchical pore structure [97,99,100]. It is worth noting that even a high-surface-area carbon product lacking multi-hierarchical porosity may not deliver efficient gas capture performance [1,101]

### 3.5. Soft Template Activation

A soft template, derived from an organic co-polymer along with carbon precursors, is employed in the preparation of meso-/macroporous carbon products [102]. This soft template results in a supramolecular arrangement, combining carbon precursors, block co-polymers, and polymers to form a mesophase. The stability of this mesophase is achieved through either a catalytic or thermal treatment. Subsequent thermal decomposition removes the template, inducing porosity in the carbon structure. To create the mesophase, a carbon donor or carbon precursor is combined with a structure-directing organic or co-polymeric agent. Both components are necessary for mesophase formation. It is crucial for the template to withstand the thermal carbonization process while also facilitating the crosslinking of carbon with polymers [102–104].

The size and morphology of carbon mesopores can be readily controlled through the implementation of soft templating effects. The creation of supramolecular products, assembled through molecular cooperation, can be regulated in terms of their size, shape, and orientation by adjusting the ratio of carbon donors to directing co-polymers [105]. Additionally, factors such as the solubility of components in the solution, the solution ratio, and polarizability effects play crucial roles in the modification of soft templating products [106,107].

The mesophase structure primarily forms through hydrogen bonding between template polymers and carbon precursors. For instance, the hydrogen-bonded molecular cooperative assembled complex of melamine and cyanuric acid (MCA), along with various other complexes like MCA and glucose (MG), Pluronic F108, Pluronic F127, P123, and ZIF-8, contribute to the formation of the mesophase structure through H-bonding [1,108,109]. Subsequent thermal treatment leads to the compaction and shrinkage of materials, resulting in the isotropic formation of mesopores ranging from 3 to 30 nm in size. The template is either partially or completely removed at temperatures between 300 and 400 °C. Simultaneously, the carbonization process also involves the aromatic polycondensation of carbon products [1,110].

## 4. Significant Role of Surface Functional Groups in Porous Carbon

The surface functional group on the carbon structure plays a critical role in CO<sub>2</sub> capture technology. Pure carbon bears adsorption energy of 6.6 kJ mol<sup>-1</sup> for CO<sub>2</sub>, which is not sufficient to capture CO<sub>2</sub> molecules and separate them from a mixture of gases (flue gas), even though CO<sub>2</sub> molecules have a higher quadrupole moment. This becomes particularly important at low pressure or during direct air capture, where higher adsorption energy is required to effectively compete with other gases and moisture [101,111]. It is essential to introduce exposed heteroatom functional groups (such as N, B, O, P, S, etc.) on the surfaces of micro-/meso-/macropores of the carbon to enhance the amount of CO<sub>2</sub> captured and the kinetics [22,112–114].

Different precursors or mixtures of hetero-precursors are utilized to prepare and induce various surface functional groups on the carbon [115,116]. Built-in functional groups efficiently improve the adsorption of CO<sub>2</sub> molecules through acid–base interactions, H-bond interactions, or electrostatic quadrupole interactions. Numerical quantification shows that O-containing, N-containing, and N-/O-co-modified functional groups on carbon improve the CO<sub>2</sub> adsorption energy to –14.3 to –22.6 kJ mol<sup>-1</sup>, –22.1 to –27.1 kJ mol<sup>-1</sup>, and –28.9 kJ mol<sup>-1</sup>, respectively [117–119].

Heteroatom doping or impregnation on the carbon structure influences its structural and mechanical stability. Heteroatom insertion counterbalances the structural or mechanical properties of the carbon by reducing the degree of polyaromatic condensation during carbonization at over 600 °C and destroying the pore structure, which poses challenges for maintaining the chemical, mechanical, and thermal stability of the carbon framework [1,120].

Xing et al. demonstrated the importance of H-bonding in N-doped activated carbon [31]. The CO<sub>2</sub> adsorption capacity is roughly proportional to the N content of the activated carbon. The presence of the N atom on the carbon lattice modifies the electronic state of the hydrogen atom in the graphene layer, intensifying the interaction between the CO<sub>2</sub> molecules and the carbon surface. The affinity for CO<sub>2</sub> molecules through H-bonding is measured by the binding energy  $\Delta E$  (kJ mol<sup>-1</sup>), where a higher value of binding energy denotes a stronger affinity for CO<sub>2</sub> molecules. A CO<sub>2</sub> molecule's binding energy without N-containing carbon is 1.26 kJ mol<sup>-1</sup>, which is much lower than the average binding energy of N-containing carbon, which is 7.84 kJ mol<sup>-1</sup>. The binding energies with NH<sub>2</sub>, pyridinic N, and CH are 11.2, 10.5, and 9.1 kJ mol<sup>-1</sup>, respectively. The findings of this study cannot correlate with or explain the traditional acid–base interaction of CO<sub>2</sub> molecules with carbon surfaces [31].

Wu et al., through DFT analysis, compared the importance of configuration types of N and O atoms in the carbon structure for the CO<sub>2</sub> physisorption mechanism on the carbon surface at the molecular level [118]; the pyridinic carbon surface shows the highest attraction to CO<sub>2</sub> molecules ( $E_{\text{ads}} = -21.4$  kJ mol<sup>-1</sup>) (Figure 9). Additionally, they explored O doping on the carbon structure, which enhances the CO<sub>2</sub> adsorption energy ( $E_{\text{ads}} = -9.7$  to  $-17.0$  kJ mol<sup>-1</sup>) compared to bare carbon ( $E_{\text{ads}} = -5.4$  kJ mol<sup>-1</sup>). They also observed a charge density difference with and without the N/O functional group, indicating no significant electron transfer between a CO<sub>2</sub> molecule and a carbon surface, which establishes physisorption as the adsorption nature of functionalized carbon.

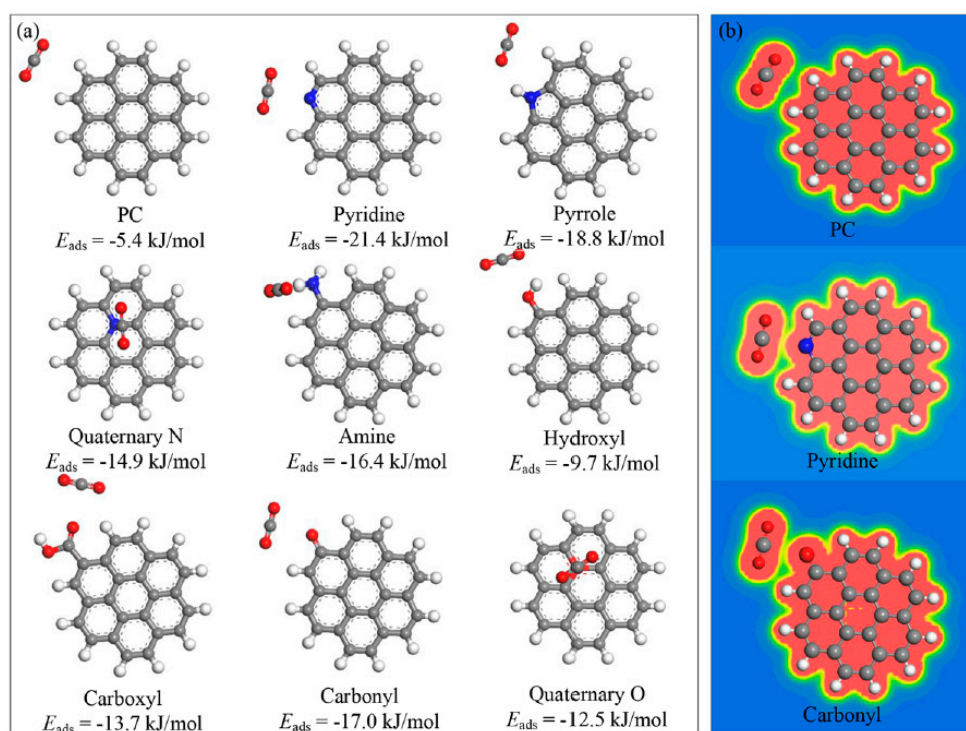


**Figure 9.** (a) CO<sub>2</sub> adsorption energy on carbon surfaces with N/O functional groups. (b) Charge density difference of CO<sub>2</sub> molecules on different carbon surfaces. C = gray; H = white; O = red; N = blue. Reprinted (adapted) with permission from [118] [Ind. Eng. Chem. Res. 2020, 59, 31, 14055–14063]. Copyright (2020) American Chemical Society.

Bari et al. investigated the precise role of surface functional groups in CO<sub>2</sub> sorption on the carbon surface using the CO<sub>2</sub> temperature-programmed desorption profile (CO<sub>2</sub>-TPD) [1]. Initially, the study adsorbed CO<sub>2</sub> at 0.2 bar and desorbed all physisorbed CO<sub>2</sub> from the porous carbon by purging with helium gas for an hour. The experiment then compared the roles of N- and O-containing functional groups in the temperature range of 50–400 °C through temperature-programmed desorption (Figure 10).

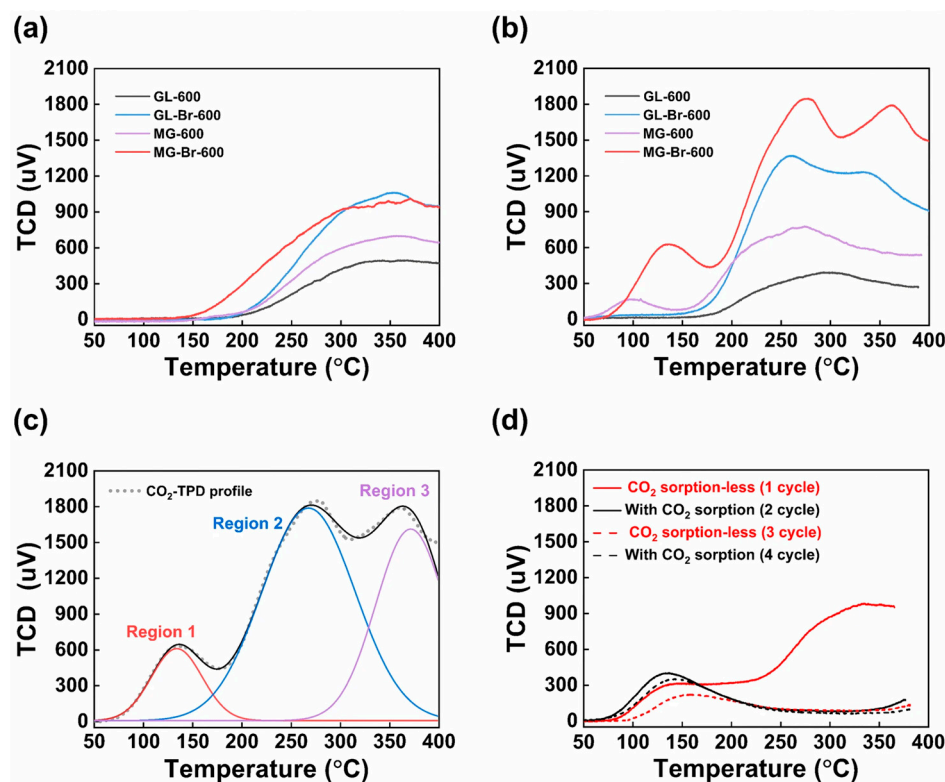


**Figure 10.** CO<sub>2</sub>-TPD profiles of carbon samples (a) without or (b) with CO<sub>2</sub> pre-adsorption, (c) deconvolution of CO<sub>2</sub>-TPD profile of MG-Br-600 with CO<sub>2</sub> pre-adsorption, and (d) multi-cycle profiles of CO<sub>2</sub>-TPD results of MG-Br-600 [1]. Adapted with permission from ref., copyright (2023) Springer Nature.

N-containing functional groups (pyridinic N, pyrrolic N, graphitic N, and oxidized N) in the carbon desorb approximately 24% of CO<sub>2</sub> within the temperature range of 60–180 °C due to weak intermolecular interactions such as hydrogen bonding, acid–amine, or electrostatic interactions. They also demonstrate that O-containing functional groups (C–OH, (CO)OR, R = H, C) act as active sites for CO<sub>2</sub> uptake by forming bicarbonate, carbamic acid, and carbamate due to strong chemical bonds ( $\sim 100$  kJ mol<sup>−1</sup>) [121]. Such chemisorbed CO<sub>2</sub> is desorbed at temperatures above 200 °C [122–124].

Jianfei et al. successfully synthesized N- and P-co-doped porous carbon by employing chitosan aerogel, phytic acid, and dicyandiamide as precursor materials. Subsequently, they activated the carbon using NaNO<sub>3</sub>, thereby circumventing the need for the utilization of harsh alkalis like NaOH or KOH (Figure 11) [125]. This innovative method yielded an impressive CO<sub>2</sub> capture performance of 5.31 mmol g<sup>−1</sup> at a pressure of 1 bar and a temperature of 25 °C. Notably, when examining the carbon sample lacking P doping, a CO<sub>2</sub> capture capacity of 1.89 mmol g<sup>−1</sup> was observed at 1 bar and 25 °C. These results strongly suggest that the synergistic interaction between N- and P-doping induces modifications in the surface chemistry, consequently augmenting the CO<sub>2</sub> capture performance [125].

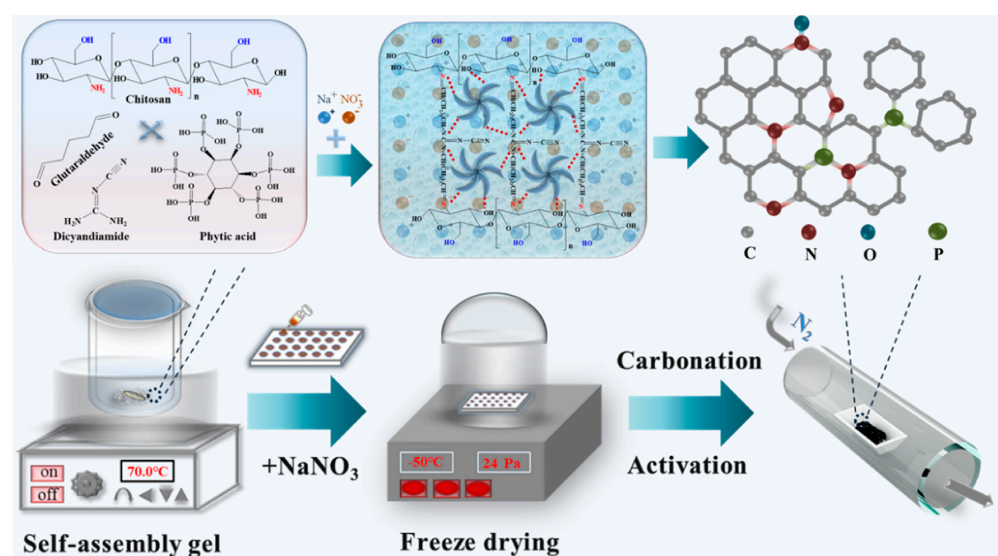


**Figure 11.** Schematic diagram of synthesis of phytic acid–induced self–assembled chitosan gel–derived N–,P–co–doped porous carbon [125]. Adapted with permission from ref., copyright (2023) Elsevier Ltd.

Similarly, Davood et al. conducted a study involving the incorporation of various heteroatoms (B, N, P, S) into activated porous carbon to enhance  $\text{CO}_2$  capture performance [126]. A comparison was made among these elements in terms of their impact. Among the considered elements (B, N, P, and S), phosphorus (P)-doping exhibited the highest efficiency in enhancing  $\text{CO}_2$  capture, yielding an uptake of  $7.13 \text{ mmol g}^{-1}$  at 1 bar and  $20^\circ\text{C}$  (Figure 12a). In this context, it is worth noting that the carbon atom (C) has a higher electronegativity (2.5) than the phosphorus (P) atom (2.1), which stands in contrast to the situation in C–N interactions, where the nitrogen (N) atom possesses an electronegativity of 3.0. This discrepancy results in the phosphorus atom displaying a relatively more positive electrostatic charge, while the carbon atom withdraws bonding electrons. Simultaneously, due to the larger atomic radius of phosphorus, the graphene structure of carbon experiences more significant distortion upon interaction. The distribution of the highest occupied molecular orbital (HOMO) and lowest unoccupied molecular orbital (LUMO) is predominantly centered around the phosphorus atom. This arrangement greatly facilitates Lewis acid–base interactions with  $\text{CO}_2$  molecules, thereby contributing significantly to the overall  $\text{CO}_2$  capture performance [126].

A hydrochar-based carbon material was synthesized through the combination of glucose and ethylene diamine, and it exhibited efficient  $\text{CO}_2$  capture performance compared to carbon derived from urea activation by KOH and carbon derived from urea activation by ZIF8, specifically in the low-pressure range of 0 to 1 bar (Figure 12b) [127]. To assess the influence of pore structure and chemical properties on  $\text{CO}_2$  adsorption capacity, a machine learning approach was employed using a dataset comprising 1594  $\text{CO}_2$  adsorption data points. The findings of the study highlight that, under low-pressure conditions (0.1–1 bar), ultra-micropores and carbon-containing nitrogen (N) functional groups have the most significant impact on  $\text{CO}_2$  capture performance (Figure 12c,d). As the pore size increases, the amount of  $\text{CO}_2$  adsorption decreases, as smaller pore sizes provide a greater likelihood of interaction between the pore walls and  $\text{CO}_2$  molecules. Notably, the machine learning outcomes emphasize that pore sizes smaller than 0.7 nm play a critical role in capturing  $\text{CO}_2$  at 1 bar. Regarding functional groups, N-containing groups such as pyridinic N, pyrrolic N, and quaternary N exhibit substantial effects on  $\text{CO}_2$  uptake, surpassing the effects of O-containing functional groups like hydroxyls, carboxylic acids, and ketones [127].

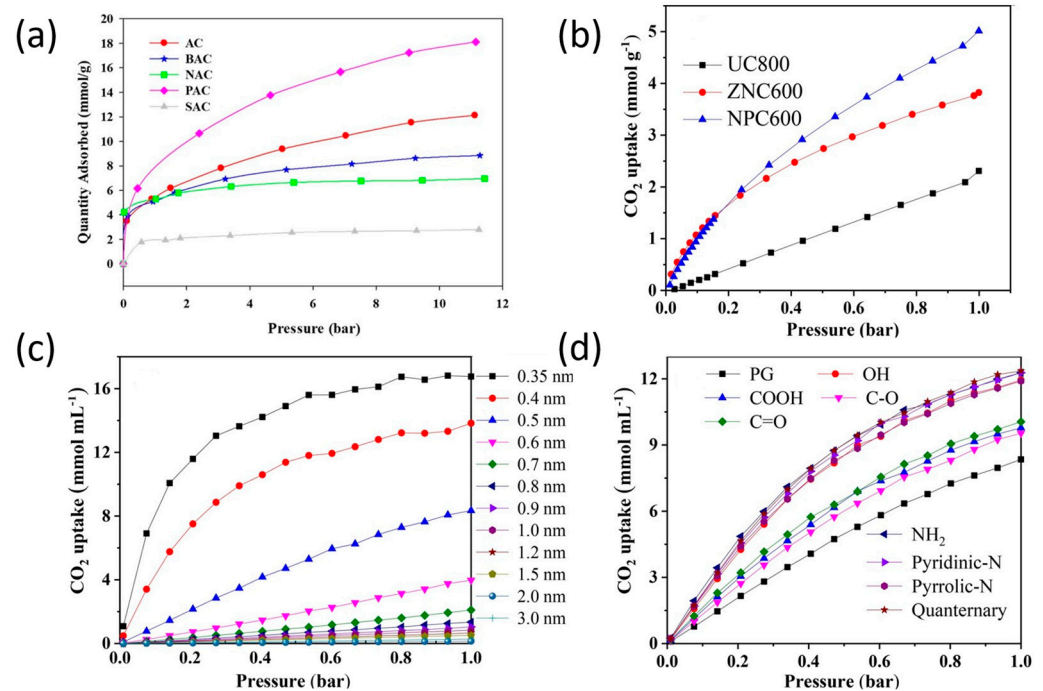


**Figure 12.** (a) CO<sub>2</sub> adsorption isotherms; AC: activated carbon; BAC, NAC, PAC, and SAC are B-, N-, P-, and S-doped activated carbon, consecutively [126]; (b) CO<sub>2</sub> adsorption isotherms; UC800: carbon from urea activated by KOH; ZNC600: carbon from urea activated by ZIF8; NPC600: hydrochar from glucose, ethylenediamine; (c) CO<sub>2</sub> adsorption isotherms of different pore size; and (d) CO<sub>2</sub> adsorption isotherms of different oxygen and nitrogen groups with 0.5 nm pore size at 25 °C [127]. Adapted with permission from refs., copyright (2023) Elsevier Ltd.

### 5. Envisioning Future Research Prospects and Forging a Focused Strategy

It is interesting to note that, until now, the development of multi-hierarchical porous carbon has mainly focused on powder-based highly efficient carbon products (Table 1).

**Table 1.** Performance comparison of CO<sub>2</sub> uptake, kinetics, heat of adsorption, and selectivity in carbon materials from different sources and under various modification processes for carbon capture.

Activation Process	Carbon Materials	Uptake (1 bar) [mmol g <sup>-1</sup> ]	Kinetics/Heat of Adsorption (Q <sub>st</sub> ) [kJ mol <sup>-1</sup> ]	Selectivity CO <sub>2</sub> /N <sub>2</sub> (15:85)	Ref.
MS/organic template	N-/O-rich multi-hierarchical porous C	3.8 (0 °C), 2.9 (25 °C)	Kinetics (Initial $k_{pi}$ , 0.2 mmol g <sup>-1</sup> min <sup>-0.5</sup> ) 26	43 (25 °C), 31 (0 °C)	[1]
Activation free	C (spherical)	2.9 (25 °C), 4 (0 °C)	27.5–29.3	CO <sub>2</sub> /N <sub>2</sub> (15/85) 30 (25 °C)	[128]
Template free	B-/N-co-doped C	2.1 (30 °C)	28	–	[129]
Chemical activation	C from industrial biomass	4.2 (25 °C), 6.6 (0 °C), 1.3 (0.15 bar)	34–18	27	[130]
Chemical activation	Defluorinated porous C	5.0 (25 °C), 8.8 (0 °C)	27.3 (zero coverage)	23 (25 °C), 22 (0 °C)	[42]

Table 1. Cont.

Activation Process	Carbon Materials	Uptake (1 bar) [mmol g <sup>-1</sup> ]	Kinetics/Heat of Adsorption (Q <sub>st</sub> ) [kJ mol <sup>-1</sup> ]	Selectivity CO <sub>2</sub> /N <sub>2</sub> (15:85)	Ref.
Template free	N-containing C (PAN)	2.4 (25 °C)	–	Simulated flue gas CO <sub>2</sub> /N <sub>2</sub> (10/90) 0.8 mmol g <sup>-1</sup> (25 °C)	[131]
Chemical activation	N-containing porous C	3.7 (25 °C), 6.2 (0 °C), 3.2 (0 °C)	15–36	18 kJ mol <sup>-1</sup> (25 °C) 129 kJ mol <sup>-1</sup> (25 °C)	[132]
Air activation	N-containing porous C fiber	2.2 (25 °C)	26.6–30.8	183	[133]
Template free	Nanoporous C	2.7 (25 °C), 4.0 (0 °C)	31.5	30	[134]
Chemical activation	N-containing porous C fiber	5.0 (25 °C), 1.5 (0.15 bar)	24.6–25.5	24	[135]
Silica template	Porous C	2.2 (25 °C)	31.8	–	[136]
Chemical activation	Porous N-containing C	2.7 (25 °C), 3.8 (25 °C)	~36	CO <sub>2</sub> /N <sub>2</sub> (10/90) 134	[137]
Freeze drying/plasma treatment	N-/O-containing porous C	0.9 (30 °C)	–	15	[118]
Ice/silica/CO <sub>2</sub> templating	N-/O-containing porous C	3.7 (25 °C)	–	–	[138]
Chemical activation	Polybenzoxazine- based porous C	8.4 (25 °C)	32–35	CO <sub>2</sub> /N <sub>2</sub> (10/90) 25 (25 °C), 34 (0 °C)	[139]
Hard template	N-containing carbon nitride	2.0 (25 °C), 2.5 (0 °C)	–	–	[140]
Template free	Ionic liquid/graphene aerogel	0.2 (0 °C)	–	CO <sub>2</sub> /CH <sub>4</sub> (ideal selectivity) 120 (25 °C), 1 mbar	[141]
Metal ion activation	N-containing porous C nanosheet	2.5 (25 °C)	–	17.5 (25 °C)	[142]
Hard template	Porous carbon from MOF	~2.5 (27 °C)	–	–	[143]
Salt template	N-containing C	3.3 (25 °C)	—	–	[144]
Template free	N-containing C monolith	3.3 (25 °C), 5 (0 °C)	~20	CO <sub>2</sub> /N <sub>2</sub> (14/86) 16 min breakthrough time (25 °C)	[26]
Chemical activation	N-containing porous C	4.0 (25 °C), 6.0 (0 °C)	~25	CO <sub>2</sub> /N <sub>2</sub> (10/90) 19 (25 °C)	[145]
Hard template	N-based porous polymer	1.0 (25 °C), 1.6 (0 °C)	–	63 (25 °C, 1 bar)	[146]

Abbreviations: Carbon is denoted as C and Molten salt as MS in the Table.

However, for practical industrial-scale applications, it is necessary to shape the powder into pellets [147]. Achieving a well-defined fixed shape and particle size before practical application requires additional fabrication steps, such as extrusion, granulation, pressing, and binder inclusion [148].

After shaping the powder into fixed pellets for practical use, there is a high concern for pressure drops across the reactor bed, which can limit mass and heat transfer [149–152]. Moreover, the inclusion of a binder or other fabrication processes can lead to changes or reductions in surface area, pore size, and pore volume [153–155]. This can also cause a significant reduction in the amount of active components and efficient functional activity, thereby affecting structural and material stability [156,157].

To overcome these drawbacks, research trends require a shift towards a pelletization-based synthesis strategy as the ultimate solution to obtain well-preserved fixed-shaped and

functionally hierarchical porous carbon products [158,159]. However, only a few research efforts have focused on this approach, and they are still far from achieving practical efficient performance [160].

It could be assumed that pelletized-state carbonization, rather than powder state carbonization or pyrolysis, will effectively improve, modify, or influence the morphological state of carbon products, due to the close contact with the carbon intermediate. It could also be assumed that the gas template is more aggressively utilized at the molecular level during the precursor's carbonization.

Figure 13 shows that, when precursors are carbonized at higher temperatures in powder form, the self-degraded or mass-loss gas template may be able to escape easily from the pyrolyzed medium. On the other hand, in a close-packed or void-filling state, the degradation products of the gas template interact more intensely and effectively at the molecular level, occupying the space left by the mass loss and providing more efficient textural properties. The proposed synthesis mechanism could reduce the technical complexity of activation by chemical or secondary physical activation (hard template, soft organic template, steam, air,  $\text{NH}_3$ , He, Ar, etc.) processes. Alternatively, it could be combined with the existing processes to explore new possibilities for obtaining more efficient carbon products.

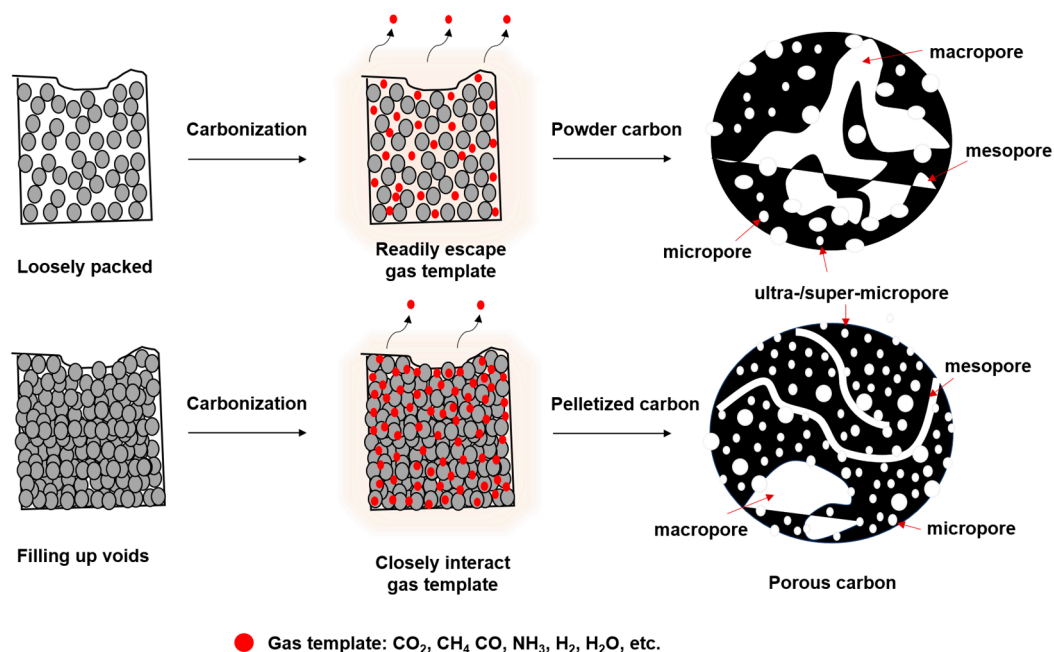


**Figure 13.** A schematic representation comparing powder and fixed-shape state carbonization strategies for the effective utilization of the gas template from the carbon degradation products.

Different activation processes come with their own set of advantages and disadvantages (Table 2). Achieving a multi-hierarchical porous carbon is crucial when considering  $\text{CO}_2$  capture efficiency, selectivity, kinetics, and a wide pressure range (including DAC, medium, and high pressures). To optimize low-pressure capture efficiency, an abundance of ultra-to-super-micropores is highly anticipated, while high-pressure scenarios tend to benefit from the presence of meso-/macropores.

To ensure both swift capture efficiency and effective utilization of ultra-micropores, it is essential to integrate them harmoniously with meso-/macropores in the overall morphological design or engineering. Furthermore, the inclusion of heteroatom-containing compositions is paramount in creating an efficient and selective adsorbent, leveraging surface chemistry. This task is challenging, as it requires the introduction of functional groups while maintaining a high degree of aromatic condensation within carbon products, in order to achieve a structurally stable carbon end-product. Combining all necessary conditions within a single-pot synthesis strategy proves to be a formidable challenge, both

in terms of attainment and the engineering of an efficient pore structure. Combining metal ion activation with soft templating and pelletization followed by carbonization in a one-pot process has the potential to produce multi-hierarchical carbon products.

**Table 2.** A comparison of the different activation processes.

Carbon Structure Modification	Advantages	Disadvantages
Chemical activation	Provides ultra pores, micropores, lower activation temperature	Extra steps of washing to remove corrosive chemicals
Physical activation	Provides micro-/meso-/macropores, readily utilized on carbonization	Cannot provide shaped carbon, higher activation temperature
Metal ion activation	Ultra-to-super-micropores	Limited carbon source, extra process of washing to remove metal
Hard template	Mechanical and structural stability, micro-/mesopores	Extra process to remove template, etching, time-consuming, can damage carbon structure due to vigorous acid or base treatment to remove template
Soft template	Self-removal with carbonization, provides multi-shaped carbon	Only meso-/macroporous carbon synthesis, template needs to remain stable during thermal process, template preparation process requires time, meso-/macropores only

## 6. Summary

Porous carbon-based materials surpass many limitations and exhibit outstanding CO<sub>2</sub> adsorption/desorption capabilities, as well as excellent clean surface cycling durability, mechanical strength, chemical resistance, and moisture stability. Various fundamental strategies have been developed to induce the efficient formation of hierarchical porous carbon products. However, applying different pressure ranges to capture CO<sub>2</sub> within multi-porosity structures poses a challenging task. This is because ultra-/super-micropores are favorable for low-pressure and low-quantity CO<sub>2</sub> adsorption, while meso-/macropores are more suited for high-pressure conditions.

Additionally, when considering the selectivity of ultra-to-micropores for CO<sub>2</sub> adsorption, the meso-/macropores region competes with other gases. Considering the molecular sieve effects, even with a higher surface area and a large number of ultra-/super-micropores, there is an unfortunate limitation in their ability to provide effective adsorption and proper kinetics due to improper diffusion pathways. Therefore, it becomes essential to devise a proper and rational design strategy to achieve a multi-hierarchical pore structure encompassing macro-/meso-/micro-/super-/ultra-pores. Moreover, the use of heteroatom-containing sources, along with inappropriate strategies for activation and templating, hinders the degree of aromatic condensation during carbonization, leading to unbalanced formation of macro-/mesopores.

The concept of merging soft templates and metal ion activation, alongside the innovative pelletization method, holds the prospect of promising potential across a diverse spectrum of practical applications (Figure 14). The ability of a soft template to direct the structure helps in incorporating heteroatoms into the carbon structure from diverse multi-component precursor sources. This plays a crucial role in maintaining the appropriate level of carbon polycondensation during the carbonization process, contributing to the mechanical strength of the structure and facilitating the development of meso- and macropores. The effectiveness of capturing CO<sub>2</sub> and performing low-pressure capture relies on the presence of ultra-to-super-micropores. Metal ion activation, in this context, facilitates the efficient creation of these ultra-to-super-micropores within the structure. Additionally, the challenges related to structural and functional degradation that often arise when shaping synthesized efficient powder for application can effectively be addressed through the proposed pre-pelletization strategy. It can be inferred that the pre-pelletization strategy makes effective use of gas templates, which share similarities with the physical activation strategy.

This approach holds the potential to provide a solution to the limitations associated with post-synthesis shaping while preserving the desired structural and functional attributes.

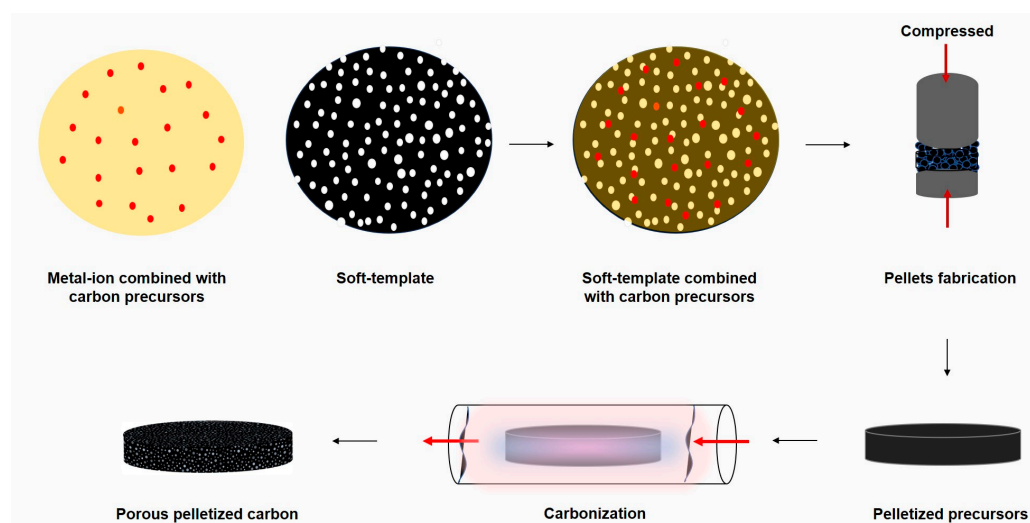


**Figure 14.** Charting a potential route: pathways to crafting pelletized porous carbon.

**Author Contributions:** Conceptualization: G.A.K.M.R.B. and J.-H.J.; Methodology: G.A.K.M.R.B.; Validation: G.A.K.M.R.B. and J.-H.J.; Writing—Original Draft: G.A.K.M.R.B.; Writing—Review and Editing: G.A.K.M.R.B. and J.-H.J.; Resources: G.A.K.M.R.B. and J.-H.J.; Supervision: G.A.K.M.R.B. and J.-H.J.; Funding Acquisition: J.-H.J. All authors have read and agreed to the published version of the manuscript.

**Funding:** This work was supported by the Korea Institute of Energy Technology Evaluation and Planning (KETEP) grant funded by the Korean government (MOTIE) (20223030020070, Development of an X-ray-based non-destructive inspection platform for maintaining the blade lightning system), and also supported by the Korea Institute of Energy Technology Evaluation and Planning (KETEP) grant funded by the Korean government (MOTIE) (2021202080023B, Development and demonstration of thermoelectric power generation system for marine application by waste heat utilization).

**Institutional Review Board Statement:** Not applicable.

**Informed Consent Statement:** Not applicable.

**Data Availability Statement:** Not applicable.

**Conflicts of Interest:** The authors declare no conflict of interest.

## References

1. Bari, G.A.R.; Kang, H.J.; Lee, T.G.; Hwang, H.J.; An, B.H.; Seo, H.W.; Ko, C.H.; Hong, W.H.; Jun, Y.S. Dual-templating-derived porous carbons for low-pressure CO<sub>2</sub> capture. *Carbon Lett.* **2023**, *33*, 811–822. [[CrossRef](#)]
2. Singh, G.; Lee, J.; Karakoti, A.; Bahadur, R.; Yi, J.; Zhao, D.; AlBahily, K.; Vinu, A. Emerging trends in porous materials for CO<sub>2</sub> capture and conversion. *Chem. Soc. Rev.* **2020**, *49*, 4360–4404. [[CrossRef](#)]
3. Ahmad, H.H.; Saleem, F.; Arif, H. Evaluation of Catastrophic Global Warming due to Coal Combustion, Paradigm of South Asia. *Int. J. Innov. Sci. Technol.* **2021**, *3*, 198–207. [[CrossRef](#)]
4. Pedraza, J.; Zimmermann, A.; Tobon, J.; Schomäcker, R.; Rojas, N. On the road to net zero-emission cement: Integrated assessment of mineral carbonation of cement kiln dust. *Chem. Eng. J.* **2021**, *408*, 127346. [[CrossRef](#)]
5. Janakiram, S.; Santinelli, F.; Costi, R.; Lindbräthen, A.; Nardelli, G.M.; Milkowski, K.; Ansaloni, L.; Deng, L. Field trial of hollow fiber modules of hybrid facilitated transport membranes for flue gas CO<sub>2</sub> capture in cement industry. *Chem. Eng. J.* **2021**, *413*, 127405. [[CrossRef](#)]
6. Fujikawa, S.; Selyanchyn, R.; Kunitake, T. A new strategy for membrane-based direct air capture. *Polym. J.* **2021**, *53*, 111–119. [[CrossRef](#)]
7. Rochelle, G.T. Amine Scrubbing for CO<sub>2</sub> Capture. *Science* **2009**, *325*, 1652–1654. [[CrossRef](#)] [[PubMed](#)]
8. Singh, A.; Sharma, Y.; Wupadrasta, Y.; Desai, K. Selection of amine combination for CO<sub>2</sub> capture in a packed bed scrubber. *Resour. -Effic. Technol.* **2016**, *2*, S165–S170. [[CrossRef](#)]

9. Li, X.; Wang, S.; Chen, C. Experimental study of energy requirement of CO<sub>2</sub> desorption from rich solvent. *Energy Procedia* **2013**, *37*, 1836–1843. [[CrossRef](#)]
10. Patel, H.A.; Byun, J.; Yavuz, C.T. Carbon Dioxide Capture Adsorbents: Chemistry and Methods. *ChemSusChem* **2017**, *10*, 1303–1317. [[CrossRef](#)] [[PubMed](#)]
11. Gao, W.; Liang, S.; Wang, R.; Jiang, Q.; Zhang, Y.; Zheng, Q.; Xie, B.; Toe, C.Y.; Zhu, X.; Wang, J.; et al. Industrial carbon dioxide capture and utilization: State of the art and future challenges. *Chem. Soc. Rev.* **2020**, *49*, 8584–8686. [[CrossRef](#)]
12. Wang, M.; Joel, A.S.; Ramshaw, C.; Eimer, D.; Musa, N.M. Process intensification for post-combustion CO<sub>2</sub> capture with chemical absorption: A critical review. *Appl. Energy* **2015**, *158*, 275–291. [[CrossRef](#)]
13. Zhang, S.; Du, M.; Shao, P.; Wang, L.; Ye, J.; Chen, J.; Chen, J. Carbonic Anhydrase Enzyme-MOFs Composite with a Superior Catalytic Performance to Promote CO<sub>2</sub> Absorption into Tertiary Amine Solution. *Environ. Sci. Technol.* **2018**, *52*, 12708–12716. [[CrossRef](#)]
14. Luis, P. Use of monoethanolamine (MEA) for CO<sub>2</sub> capture in a global scenario: Consequences and alternatives. *Desalination* **2016**, *380*, 93–99. [[CrossRef](#)]
15. MacDowell, N.; Florin, N.; Buchard, A.; Hallett, J.; Galindo, A.; Jackson, G.; Adjiman, C.S.; Williams, C.K.; Shah, N.; Fennell, P. An overview of CO<sub>2</sub> capture technologies. *Energy Environ. Sci.* **2010**, *3*, 1645–1669. [[CrossRef](#)]
16. Sabatino, F.; Grimm, A.; Gallucci, F.; van Sint Annaland, M.; Kramer, G.J.; Gazzani, M. A comparative energy and costs assessment and optimization for direct air capture technologies. *Joule* **2021**, *5*, 2047–2076. [[CrossRef](#)]
17. Barzagli, F.; Mani, F.; Peruzzini, M. A Comparative Study of the CO<sub>2</sub> Absorption in Some Solvent-Free Alkanolamines and in Aqueous Monoethanolamine (MEA). *Environ. Sci. Technol.* **2016**, *50*, 7239–7246. [[CrossRef](#)]
18. Mazari, S.A.; Ali, B.S.; Jan, B.M.; Saeed, I.M. Degradation study of piperazine, its blends and structural analogs for CO<sub>2</sub> capture: A review. *Int. J. Greenh. Gas Control* **2014**, *31*, 214–228. [[CrossRef](#)]
19. Chang, B.; Shi, W.; Yin, H.; Zhang, S.; Yang, B. Poplar catkin-derived self-templated synthesis of N-doped hierarchical porous carbon microtubes for effective CO<sub>2</sub> capture. *Chem. Eng. J.* **2019**, *358*, 1507–1518. [[CrossRef](#)]
20. Oschatz, M.; Antonietti, M. A search for selectivity to enable CO<sub>2</sub> capture with porous adsorbents. *Energy Environ. Sci.* **2018**, *11*, 57–70. [[CrossRef](#)]
21. Wang, X.; He, T.; Hu, J.; Liu, M. The progress of nanomaterials for carbon dioxide capture via the adsorption process. *Environ. Sci. Nano.* **2021**, *8*, 890–912. [[CrossRef](#)]
22. Zhang, Z.; Cano, Z.P.; Luo, D.; Dou, H.; Yu, A.; Chen, Z. Rational design of tailored porous carbon-based materials for CO<sub>2</sub> capture. *J. Mater. Chem. A Mater.* **2019**, *7*, 20985–21003. [[CrossRef](#)]
23. Sukor, N.R.; Shamsuddin, A.H.; Mahlia, T.M.I.; Isa, M.F.M. Techno-economic analysis of CO<sub>2</sub> capture technologies in offshore natural gas field: Implications to carbon capture and storage in Malaysia. *Processes* **2020**, *8*, 350. [[CrossRef](#)]
24. Micari, M.; Dakhchoune, M.; Agrawal, K.V. Techno-economic assessment of postcombustion carbon capture using high-performance nanoporous single-layer graphene membranes. *J. Memb. Sci.* **2021**, *624*, 119103. [[CrossRef](#)]
25. John, J.M.; Alwi, S.R.W.; Omoregbe, D.I. Techno-economic analysis of carbon dioxide capture and utilisation analysis for an industrial site with fuel cell integration. *J. Clean. Prod.* **2021**, *281*, 124920. [[CrossRef](#)]
26. Hao, G.P.; Li, W.C.; Qian, D.; Wang, G.H.; Zhang, W.P.; Zhang, T.; Wang, A.Q.; Schüth, F.; Bongard, H.J.; Lu, A.H. Structurally designed synthesis of mechanically stable poly(benzoxazine-co-resol)-based porous carbon monoliths and their application as high-performance CO<sub>2</sub> capture sorbents. *J. Am. Chem. Soc.* **2011**, *133*, 11378–11388. [[CrossRef](#)] [[PubMed](#)]
27. Ray, B.; Churipard, S.R.; Peter, S.C. An overview of the materials and methodologies for CO<sub>2</sub> capture under humid conditions. *J. Mater. Chem. A Mater.* **2021**, *9*, 26498–26527. [[CrossRef](#)]
28. Zhao, Y.; Yao, K.X.; Teng, B.; Zhang, T.; Han, Y. A perfluorinated covalent triazine-based framework for highly selective and water-tolerant CO<sub>2</sub> capture. *Energy Environ. Sci.* **2013**, *6*, 3684–3692. [[CrossRef](#)]
29. Masala, A.; Vitillo, J.G.; Mondino, G.; Grande, C.A.; Blom, R.; Manzoli, M.; Marshall, M.; Bordiga, S. CO<sub>2</sub> capture in dry and wet conditions in UTSA-16 metal-organic framework. *ACS Appl. Mater. Interfaces* **2017**, *9*, 455–463. [[CrossRef](#)]
30. Yang, J.; Yue, L.; Hu, X.; Wang, L.; Zhao, Y.; Lin, Y.; Sun, Y.; DaCosta, H.; Guo, L. Efficient CO<sub>2</sub> Capture by Porous Carbons Derived from Coconut Shell. *Energy Fuels* **2017**, *31*, 4287–4293. [[CrossRef](#)]
31. Xing, W.; Liu, C.; Zhou, Z.; Zhang, L.; Zhou, J.; Zhuo, S.; Yan, Z.; Gao, H.; Wang, G.; Qiao, S.Z. Superior CO<sub>2</sub> uptake of N-doped activated carbon through hydrogen-bonding interaction. *Energy Environ. Sci.* **2012**, *5*, 7323–7327. [[CrossRef](#)]
32. Sevilla, M.; Fuertes, A.B. Sustainable porous carbons with a superior performance for CO<sub>2</sub> capture. *Energy Environ. Sci.* **2011**, *4*, 1765–1771. [[CrossRef](#)]
33. To, J.W.; He, J.; Mei, J.; Haghpanah, R.; Chen, Z.; Kurosawa, T.; Chen, S.; Bae, W.G.; Pan, L.; Tok, J.B.H.; et al. Hierarchical N-Doped Carbon as CO<sub>2</sub> Adsorbent with High CO<sub>2</sub> Selectivity from Rationally Designed Polypyrrole Precursor. *J. Am. Chem. Soc.* **2016**, *138*, 1001–1009. [[CrossRef](#)] [[PubMed](#)]
34. Creamer, A.E.; Gao, B. Carbon-based adsorbents for postcombustion CO<sub>2</sub> capture: A critical review. *Environ. Sci. Technol.* **2016**, *50*, 7276–7289. [[CrossRef](#)]
35. Yang, I.; Jung, M.; Kim, M.S.; Choi, D.; Jung, J.C. Physical and chemical activation mechanisms of carbon materials based on the microdomain model. *J. Mater. Chem. A Mater.* **2021**, *9*, 9815–9825. [[CrossRef](#)]
36. Quan, C.; Zhou, Y.; Wang, J.; Wu, C.; Gao, N. Biomass-based carbon materials for CO<sub>2</sub> capture: A review. *J. CO<sub>2</sub> Util.* **2023**, *68*, 102373. [[CrossRef](#)]

37. Malini, K.; Selvakumar, D.; Kumar, N.S. Activated carbon from biomass: Preparation, factors improving basicity and surface properties for enhanced CO<sub>2</sub> capture capacity—A review. *J. CO<sub>2</sub> Util.* **2023**, *67*, 102318. [[CrossRef](#)]
38. Xing, W.; Liu, C.; Zhou, Z.; Zhou, J.; Wang, G.; Zhuo, S.; Xue, Q.; Song, L.; Yan, Z. Oxygen-containing functional group-facilitated CO<sub>2</sub> capture by carbide-derived carbons. *Nanoscale Res. Lett.* **2014**, *9*, 189. [[CrossRef](#)]
39. Khosrowshahi, M.S.; Abdol, M.A.; Mashhadimoslem, H.; Khakpour, E.; Emrooz, H.B.M.; Sadeghzadeh, S.; Ghaemi, A. The role of surface chemistry on CO<sub>2</sub> adsorption in biomass-derived porous carbons by experimental results and molecular dynamics simulations. *Sci. Rep.* **2022**, *12*, 8917. [[CrossRef](#)]
40. Wang, T.; Wang, X.; Hou, C.; Liu, J. Quaternary functionalized mesoporous adsorbents for ultra-high kinetics of CO<sub>2</sub> capture from air. *Sci. Rep.* **2020**, *10*, 21429. [[CrossRef](#)]
41. Yang, Y.B.; Hao, Q.; Müller-Plathe, F.; Böhm, M.C. Monte Carlo Simulations of SO<sub>2</sub>, H<sub>2</sub>S, and CO<sub>2</sub> Adsorption in Charged Single-Walled Carbon Nanotube Arrays. *J. Phys. Chem. C* **2020**, *124*, 5838–5852. [[CrossRef](#)]
42. Wang, R.; Xi, S.C.; Wang, D.Y.; Dou, M.; Dong, B. Defluorinated Porous Carbon Nanomaterials for CO<sub>2</sub> Capture. *ACS Appl. Nano Mater.* **2021**, *4*, 10148–10154. [[CrossRef](#)]
43. Hu, M.; He, J.; Zhao, Z.; Strobel, T.A.; Hu, W.; Yu, D.; Sun, H.; Liu, L.; Li, Z.; Ma, M.; et al. Compressed glassy carbon: An ultrastrong and elastic interpenetrating graphene network. *Sci. Adv.* **2017**, *3*, 3213. [[CrossRef](#)]
44. Mao, H.; Tang, J.; Chen, J.; Wan, J.; Hou, K.; Peng, Y.; Halat, D.M.; Xiao, L.; Zhang, R.; Lv, X.; et al. Designing hierarchical nanoporous membranes for highly efficient gas adsorption and storage. *Sci. Adv.* **2020**, *6*, eabb0694. [[CrossRef](#)]
45. Park, J.W.; Hwang, H.J.; Kang, H.J.; Bari, G.A.R.; Lee, T.G.; An, B.H.; Cho, S.Y.; Jun, Y.S. Hierarchical porous, N-containing carbon supports for high loading sulfur cathodes. *Nanomaterials* **2021**, *11*, 408. [[CrossRef](#)]
46. Wang, R.; Jia, J.; Jin, Q.; Chen, H.; Liu, H.; Yin, Q.; Zhao, Z. Forming mechanism of coke microparticles from polymerization of aqueous organics during hydrothermal carbonization process of biomass. *Carbon* **2022**, *192*, 50–60. [[CrossRef](#)]
47. Hao, W.; Björkman, E.; Lilliestråle, M.; Hedin, N. Activated carbons prepared from hydrothermally carbonized waste biomass used as adsorbents for CO<sub>2</sub>. *Appl. Energy* **2013**, *112*, 526–532. [[CrossRef](#)]
48. Zhuang, X.; Liu, J.; Zhang, Q.; Wang, C.; Zhan, H.; Ma, L. A review on the utilization of industrial biowaste via hydrothermal carbonization. *Renew. Sustain. Energy Rev.* **2022**, *154*, 111877. [[CrossRef](#)]
49. Silva, F.V.E.; Monteggia, L.O. Pyrolysis of algal biomass obtained from high-rate algae ponds applied to wastewater treatment. *Front. Energy Res.* **2015**, *3*, 31. [[CrossRef](#)]
50. Wang, S.; Zhang, H.; Huang, H.; Xiao, R.; Li, R.; Zhang, Z. Influence of temperature and residence time on characteristics of biochars derived from agricultural residues: A comprehensive evaluation. *Process Saf. Environ. Prot.* **2020**, *139*, 218–229. [[CrossRef](#)]
51. Falco, C.; Baccile, N.; Titirici, M.M. Morphological and structural differences between glucose, cellulose and lignocellulosic biomass derived hydrothermal carbons. *Green Chem.* **2011**, *13*, 3273–3281. [[CrossRef](#)]
52. Kang, H.J.; Bari, G.A.R.; Lee, T.G.; Khan, T.T.; Park, J.W.; Hwang, H.J.; Cho, S.Y.; Jun, Y.S. Microporous carbon nanoparticles for lithium-sulfur batteries. *Nanomaterials* **2020**, *10*, 2012. [[CrossRef](#)]
53. Sekirifa, M.L.; Hadj-Mahammed, M.; Pallier, S.; Baameur, L.; Richard, D.; Al-Dujaili, A.H. Preparation and characterization of an activated carbon from a date stones variety by physical activation with carbon dioxide. *J. Anal. Appl. Pyrolysis.* **2013**, *99*, 155–160. [[CrossRef](#)]
54. Ogungbenro, A.E.; Quang, D.V.; Al-Ali, K.A.; Vega, L.F.; Abu-Zahra, M.R.M. Physical synthesis and characterization of activated carbon from date seeds for CO<sub>2</sub> capture. *J. Environ. Chem. Eng.* **2018**, *6*, 4245–4252. [[CrossRef](#)]
55. Singh, G.; Lakhi, K.S.; Sil, S.; Bhosale, S.V.; Kim, I.; Albahily, K.; Vinu, A. Biomass derived porous carbon for CO<sub>2</sub> capture. *Carbon* **2019**, *148*, 164–186. [[CrossRef](#)]
56. Kupgan, G.; Liyana-Arachchi, T.P.; Colina, C.M. NLDFT Pore Size Distribution in Amorphous Microporous Materials. *Langmuir* **2017**, *33*, 11138–11145. [[CrossRef](#)]
57. Dantas, S.; Struckhoff, K.C.; Thommes, M.; Neimark, A.V. Pore size characterization of micro-mesoporous carbons using CO<sub>2</sub> adsorption. *Carbon* **2021**, *173*, 842–848. [[CrossRef](#)]
58. Sanz-Pérez, E.S.; Murdock, C.R.; Didas, S.A.; Jones, C.W. Direct Capture of CO<sub>2</sub> from Ambient Air. *Chem. Rev.* **2016**, *116*, 11840–11876. [[CrossRef](#)]
59. Mehio, N.; Dai, S.; Jiang, D.E. Quantum mechanical basis for kinetic diameters of small gaseous molecules. *J. Phys. Chem. A* **2014**, *118*, 1150–1154. [[CrossRef](#)] [[PubMed](#)]
60. Petrovic, B.; Gorbounov, M.; Soltani, S.M. Impact of Surface Functional Groups and Their Introduction Methods on the Mechanisms of CO<sub>2</sub> Adsorption on Porous Carbonaceous Adsorbents. *Carbon Capture Sci. Technol.* **2022**, *3*, 100045. [[CrossRef](#)]
61. Lim, G.; Lee, K.B.; Ham, H.C. Effect of N-Containing Functional Groups on CO<sub>2</sub> Adsorption of Carbonaceous Materials: A Density Functional Theory Approach. *J. Phys. Chem. C* **2016**, *120*, 8087–8095. [[CrossRef](#)]
62. Wang, Y.; Hu, X.; Hao, J.; Ma, R.; Guo, Q.; Gao, H.; Bai, H. Nitrogen and Oxygen Codoped Porous Carbon with Superior CO<sub>2</sub> Adsorption Performance: A Combined Experimental and DFT Calculation Study. *Ind. Eng. Chem. Res.* **2019**, *58*, 13390–13400. [[CrossRef](#)]
63. Parshetti, G.K.; Chowdhury, S.; Balasubramanian, R. Biomass derived low-cost microporous adsorbents for efficient CO<sub>2</sub> capture. *Fuel* **2015**, *148*, 246–254. [[CrossRef](#)]

64. Igalavithana, A.D.; Choi, S.W.; Shang, J.; Hanif, A.; Dissanayake, P.D.; Tsang, D.C.; Kwon, J.H.; Lee, K.B.; Ok, Y.S. Carbon dioxide capture in biochar produced from pine sawdust and paper mill sludge: Effect of porous structure and surface chemistry. *Sci. Total Environ.* **2020**, *739*, 139845. [[CrossRef](#)]
65. Zhang, Z.; Zhou, J.; Xing, W.; Xue, Q.; Yan, Z.; Zhuo, S.; Qiao, S.Z. Critical role of small micropores in high CO<sub>2</sub> uptake. *Phys. Chem. Chem. Phys.* **2013**, *15*, 2523–2529. [[CrossRef](#)]
66. Sun, N.; Sun, C.; Liu, J.; Liu, H.; Snape, C.E.; Li, K. Surface-modified spherical activated carbon materials for pre-combustion carbon dioxide capture. *RSC Adv.* **2015**, *5*, 33681–33690. [[CrossRef](#)]
67. Gao, A.; Guo, N.; Yan, M.; Li, M.; Wang, F.; Yang, R. Hierarchical porous carbon activated by CaCO<sub>3</sub> from pigskin collagen for CO<sub>2</sub> and H<sub>2</sub> adsorption. *Microporous Mesoporous Mater.* **2018**, *260*, 172–179. [[CrossRef](#)]
68. Zhang, X.; Elsayed, I.; Song, X.; Shmulsky, R.; Hassan, E.B. Microporous carbon nanoflakes derived from biomass cork waste for CO<sub>2</sub> capture. *Sci. Total Environ.* **2020**, *748*, 142465. [[CrossRef](#)]
69. Zhu, W.; Wang, Y.; Yao, F.; Wang, X.; Zheng, H.; Ye, G.; Cheng, H.; Wu, J.; Huang, H.; Ye, D. One-pot synthesis of N-doped petroleum coke-based microporous carbon for high-performance CO<sub>2</sub> adsorption and supercapacitors. *J. Environ. Sci.* **2024**, *139*, 93–104. [[CrossRef](#)]
70. Serafin, J.; Dziejarski, B.; Vendrell, X.; Kielbasa, K.; Michalkiewicz, B. Biomass waste fern leaves as a material for a sustainable method of activated carbon production for CO<sub>2</sub> capture. *Biomass Bioenergy* **2023**, *175*, 106880. [[CrossRef](#)]
71. Zhang, Z.; Luo, D.; Lui, G.; Li, G.; Jiang, G.; Cano, Z.P.; Deng, Y.P.; Du, X.; Yin, S.; Chen, Y.; et al. In-situ ion-activated carbon nanospheres with tunable ultramicroporosity for superior CO<sub>2</sub> capture. *Carbon* **2019**, *143*, 531–541. [[CrossRef](#)]
72. Sajjadi, B.; Chen, W.Y.; Egiebor, N.O. A comprehensive review on physical activation of biochar for energy and environmental applications. *Rev. Chem. Eng.* **2019**, *35*, 735–776. [[CrossRef](#)]
73. Alvim-Ferraz, M.C.M.; Gaspar, C.M.T.B. Micropore size distribution of activated carbons impregnated after carbonization. *J. Porous Mater.* **2003**, *10*, 47–55. [[CrossRef](#)]
74. Prauchner, M.J.; Sapag, K.; Rodríguez-Reinoso, F. Tailoring biomass-based activated carbon for CH<sub>4</sub> storage by combining chemical activation with H<sub>3</sub>PO<sub>4</sub> or ZnCl<sub>2</sub> and physical activation with CO<sub>2</sub>. *Carbon* **2016**, *110*, 138–147. [[CrossRef](#)]
75. Kim, H.S.; Kang, M.S.; Yoo, W.C. Highly Enhanced Gas Sorption Capacities of N-Doped Porous Carbon Spheres by Hot NH<sub>3</sub> and CO<sub>2</sub> Treatments. *J. Phys. Chem. C* **2015**, *119*, 28512–28522. [[CrossRef](#)]
76. Khuong, D.A.; Nguyen, H.N.; Tsubota, T. Activated carbon produced from bamboo and solid residue by CO<sub>2</sub> activation utilized as CO<sub>2</sub> adsorbents. *Biomass Bioenergy* **2021**, *148*, 106039. [[CrossRef](#)]
77. Rajapaksha, A.U.; Vithanage, M.; Lee, S.S.; Seo, D.C.; Tsang, D.C.W.; Ok, Y.S. Steam activation of biochars facilitates kinetics and pH-resilience of sulfamethazine sorption. *J. Soils Sediments* **2016**, *16*, 889–895. [[CrossRef](#)]
78. Fu, J.; Zhang, J.; Jin, C.; Wang, Z.; Wang, T.; Cheng, X.; Ma, C. Effects of temperature, oxygen and steam on pore structure characteristics of coconut husk activated carbon powders prepared by one-step rapid pyrolysis activation process. *Bioresour Technol* **2020**, *310*, 123413. [[CrossRef](#)]
79. Muthmann, J.; Bläker, C.; Pasel, C.; Luckas, M.; Schledorn, C.; Bathen, D. Characterization of structural and chemical modifications during the steam activation of activated carbons. *Microporous Mesoporous Mater.* **2020**, *309*, 110549. [[CrossRef](#)]
80. Heo, Y.J.; Park, S.J. A role of steam activation on CO<sub>2</sub> capture and separation of narrow microporous carbons produced from cellulose fibers. *Energy* **2015**, *91*, 142–150. [[CrossRef](#)]
81. Bardestani, R.; Kaliaguine, S. Steam activation and mild air oxidation of vacuum pyrolysis biochar. *Biomass Bioenergy* **2018**, *108*, 101–112. [[CrossRef](#)]
82. Suliman, W.; Harsh, J.B.; Abu-Lail, N.I.; Fortuna, A.M.; Dallmeyer, I.; Garcia-Perez, M. Modification of biochar surface by air oxidation: Role of pyrolysis temperature. *Biomass Bioenergy* **2016**, *85*, 1–11. [[CrossRef](#)]
83. Xiao, F.; Bedane, A.H.; Mallula, S.; Sasi, P.C.; Alinezhad, A.; Soli, D.; Hagen, Z.M.; Mann, M.D. Production of granular activated carbon by thermal air oxidation of biomass charcoal/biochar for water treatment in rural communities: A mechanistic investigation. *Chem. Eng. J. Adv.* **2020**, *4*, 100035. [[CrossRef](#)]
84. Petrovic, B.; Gorbounov, M.; Soltani, S.M. Influence of surface modification on selective CO<sub>2</sub> adsorption: A technical review on mechanisms and methods. *Microporous Mesoporous Mater.* **2021**, *312*, 110751. [[CrossRef](#)]
85. Zaker, A.; Hammouda, S.B.; Sun, J.; Wang, X.; Li, X.; Chen, Z. Carbon-based materials for CO<sub>2</sub> capture: Their production, modification and performance. *J. Environ. Chem. Eng.* **2023**, *11*, 109741. [[CrossRef](#)]
86. Zhou, J.; Li, Z.; Xing, W.; Zhu, T.; Shen, H.; Zhuo, S. N-doped microporous carbons derived from direct carbonization of K<sup>+</sup>-exchanged meta-aminophenol-formaldehyde resin for superior CO<sub>2</sub> sorption. *Chem. Commun.* **2015**, *51*, 4591–4594. [[CrossRef](#)]
87. Zhou, Z.Q.J.; Li, Z.; Xing, W.; Shen, H.; Bi, X.; Zhu, T.; Zhuo, S. A New Approach to Tuning Carbon Ultramicropore Size at Sub-Angstrom Level for Maximizing Specific Capacitance and CO<sub>2</sub> Uptake. *Adv. Funct. Mater.* **2016**, *26*, 7955–7964. [[CrossRef](#)]
88. Itoi, H.; Nishihara, H.; Kogure, T.; Kyotani, T. Three-dimensionally arrayed and mutually connected 1.2-nm nanopores for high-performance electric double layer capacitor. *J. Am. Chem. Soc.* **2011**, *133*, 1165–1167. [[CrossRef](#)]
89. Zhu, S.; Zhao, N.; Li, J.; Deng, X.; Sha, J.; He, C. Hard-template synthesis of three-dimensional interconnected carbon networks: Rational design, hybridization and energy-related applications. *Nano Today* **2019**, *29*, 100796. [[CrossRef](#)]
90. Joseph, S.; Singh, G.; Lee, J.M.; Yu, X.; Breese, M.B.; Ruban, S.M.; Bhargava, S.K.; Yi, J.; Vinu, A. Hierarchical carbon structures from soft drink for multi-functional energy applications of Li-ion battery, Na-ion battery and CO<sub>2</sub> capture. *Carbon* **2023**, *210*, 118085. [[CrossRef](#)]

91. Vilian, A.E.; Song, J.Y.; Lee, Y.S.; Hwang, S.K.; Kim, H.J.; Jun, Y.S.; Huh, Y.S.; Han, Y.K. Salt-templated three-dimensional porous carbon for electrochemical determination of gallic acid. *Biosens. Bioelectron.* **2018**, *117*, 597–604. [CrossRef]
92. Deng, X.; Zhao, B.; Zhu, L.; Shao, Z. Molten salt synthesis of nitrogen-doped carbon with hierarchical pore structures for use as high-performance electrodes in supercapacitors. *Carbon* **2015**, *93*, 48–58. [CrossRef]
93. Liu, X.; Antonietti, M. Moderating black powder chemistry for the synthesis of doped and highly porous graphene nanoplatelets and their use in electrocatalysis. *Adv. Mater.* **2013**, *25*, 6284–6290. [CrossRef]
94. Liu, X.; Giordano, C.; Antonietti, M. A facile molten-salt route to graphene synthesis. *Small* **2014**, *10*, 193–200. [CrossRef] [PubMed]
95. Fechler, N.; Fellingner, T.P.; Antonietti, M. ‘salt templating’: A simple and sustainable pathway toward highly porous functional carbons from ionic liquids. *Adv. Mater.* **2013**, *25*, 75–79. [CrossRef]
96. Yang, Z.; Xia, Y.; Sun, X.; Mokaya, R. Preparation and hydrogen storage properties of zeolite-templated carbon materials nanocast via chemical vapor deposition: Effect of the zeolite template and nitrogen doping. *J. Phys. Chem. B* **2006**, *110*, 18424–18431. [CrossRef] [PubMed]
97. Asasian-Kolur, N.; Sharifian, S.; Haddadi, B.; Jordan, C.; Harasek, M. *Ordered Porous Carbon Preparation by Hard Templating Approach for Hydrogen Adsorption Application*; Springer: Berlin/Heidelberg, Germany, 2023. [CrossRef]
98. Wang, J.; Wang, Y.; Hu, H.; Yang, Q.; Cai, J. From metal-organic frameworks to porous carbon materials: Recent progress and prospects from energy and environmental perspectives. *Nanoscale* **2020**, *12*, 4238–4268. [CrossRef]
99. Xu, X.; Xu, C.; Liu, J.; Jin, R.; Luo, X.; Shu, C.; Chen, H.; Guo, C.; Xu, L.; Si, Y. The synergistic effect of ‘soft-hard template’ to in situ regulate mass transfer and defective sites of doped-carbon nanostructures for catalysis of oxygen reduction. *J. Alloys Compd.* **2023**, *939*, 168782. [CrossRef]
100. Lee, J.; Han, S.; Hyeon, T. Synthesis of new nanoporous carbon materials using nanostructured silica materials as templates. *J. Mater. Chem.* **2004**, *14*, 478–486. [CrossRef]
101. Rehman, A.; Heo, Y.J.; Nazir, G.; Park, S.J. Solvent-free, one-pot synthesis of nitrogen-tailored alkali-activated microporous carbons with an efficient CO<sub>2</sub> adsorption. *Carbon* **2021**, *172*, 71–82. [CrossRef]
102. Shi, J.; Xu, J.; Cui, H.; Yan, N.; Zou, J.; Liu, Y.; You, S. Synthesis of highly porous N-doped hollow carbon nanospheres with a combined soft template-chemical activation method for CO<sub>2</sub> capture. *Ind. Crops Prod.* **2023**, *280*, 115952. [CrossRef]
103. Chuenchom, L.; Kraehnert, R.; Smarsly, B.M. Recent progress in soft-templating of porous carbon materials. *Soft Matter* **2012**, *8*, 10801–10812. [CrossRef]
104. Xu, Z.; Wu, Z.; Chi, J.; Lei, E.; Liu, Y.; Yin, Y.; Yang, Z.; Ma, C.; Li, W.; Luo, S.; et al. Soft-template hydrothermal synthesis of N and B co-doped walnut-shaped porous carbon spheres with hydrophilic surfaces for supercapacitors. *Appl. Surf. Sci.* **2023**, *638*, 158016. [CrossRef]
105. Kang, H.J.; Huh, Y.S.; Im, W.B.; Jun, Y.S. Molecular cooperative assembly-mediated synthesis of ultra-high-performance hard carbon anodes for dual-carbon sodium hybrid capacitors. *ACS Nano* **2019**, *13*, 11935–11946. [CrossRef] [PubMed]
106. Guan, L.; Hu, H.; Teng, X.L.; Zhu, Y.F.; Zhang, Y.L.; Chao, H.X.; Yang, H.; Wang, X.S.; Wu, M.B. Templating synthesis of porous carbons for energy-related applications: A review. *New Carbon Mater.* **2022**, *37*, 25–45. [CrossRef]
107. Jun, Y.S.; Lee, E.Z.; Wang, X.; Hong, W.H.; Stucky, G.D.; Thomas, A. From melamine-cyanuric acid supramolecular aggregates to carbon nitride hollow spheres. *Adv. Funct. Mater.* **2013**, *23*, 3661–3667. [CrossRef]
108. Nicolae, S.A.; Szilágyi, Á.; Titirici, M.M. Soft templating production of porous carbon adsorbents for CO<sub>2</sub> and H<sub>2</sub>S capture. *Carbon* **2020**, *169*, 193–204. [CrossRef]
109. Zhang, Z.; Chen, Y.; Wang, P.; Wang, Z.; Zuo, C.; Chen, W.; Ao, T. Facile fabrication of N-doped hierarchical porous carbons derived from soft-templated ZIF-8 for enhanced adsorptive removal of tetracycline hydrochloride from water. *J. Hazard Mater.* **2022**, *423*, 127103. [CrossRef]
110. Chen, L.; Yuan, Y.; Zhang, D.; Lin, Z.; Lin, J.; Li, S.; Guo, S. Construction of 3D hierarchical honeycomb macro/meso/micro-porous carbon with soft and hard templates for high-performance sodium-ion batteries. *Mater. Lett.* **2023**, *334*, 133737. [CrossRef]
111. Bin, A.A.; Binti, J.H. *Waste Recycling Technologies for Nanomaterials Manufacturing: Manufacturing of Nanoalumina by Recycling of Aluminium Cans Waste Aiman*; Springer: Cham, Switzerland, 2021. Available online: <https://link.springer.com/book/10.1007/978-3-030-68031-2> (accessed on 8 July 2023).
112. Xu, S.; Niu, M.; Zhao, G.; Ming, S.; Li, X.; Zhu, Q.; Ding, L.X.; Kim, M.; Allothman, A.A.; Mushab, M.S.S.; et al. Size control and electronic manipulation of Ru catalyst over B, N co-doped carbon network for high-performance hydrogen evolution reaction. *Nano Res.* **2023**, *16*, 6212–6219. [CrossRef]
113. Jin, X.; Wang, X.; Liu, Y.; Kim, M.; Cao, M.; Xie, H.; Liu, S.; Wang, X.; Huang, W.; Nanjundan, A.K.; et al. Nitrogen and Sulfur Co-Doped Hierarchically Porous Carbon Nanotubes for Fast Potassium Ion Storage. *Small* **2022**, *18*, 42. [CrossRef]
114. Emran, M.Y.; Shenashen, M.A.; El-Safty, S.A.; Selim, M.M. Design of porous S-doped carbon nanostructured electrode sensor for sensitive and selective detection of guanine from DNA samples. *Microporous Mesoporous Mater.* **2021**, *320*, 111097. [CrossRef]
115. Khosropour, H.; Rezaei, B.; Alinajafi, H.A.; Ensafi, A.A. Electrochemical sensor based on glassy carbon electrode modified by polymelamine formaldehyde/graphene oxide nanocomposite for ultrasensitive detection of oxycodone. *Microchimica Acta* **2021**, *188*, 1. [CrossRef]
116. Emran, M.Y.; Shenashen, M.A.; Elmarakbi, A.; Selim, M.M.; El-Safty, S.A. Nitrogen-doped carbon hollow trunk-like structure as a portable electrochemical sensor for noradrenaline detection in neuronal cells. *Anal. Chim. Acta* **2022**, *1192*, 339380. [CrossRef]

117. Wu, D.; Yang, Y.; Liu, J.; Zheng, Y. Plasma-Modified N/O-Doped Porous Carbon for CO<sub>2</sub> Capture: An Experimental and Theoretical Study. *Energy Fuels* **2020**, *34*, 6077–6084. [[CrossRef](#)]
118. Wu, D.; Liu, J.; Yang, Y.; Zheng, Y. Nitrogen/Oxygen Co-Doped Porous Carbon Derived from Biomass for Low-Pressure CO<sub>2</sub> Capture. *Ind. Eng. Chem. Res.* **2020**, *59*, 14055–14063. [[CrossRef](#)]
119. Ashourirad, B.; Arab, P.; Islamoglu, T.; Cychosz, K.A.; Thommes, M.; El-Kaderi, H.M. A cost-effective synthesis of heteroatom-doped porous carbons as efficient CO<sub>2</sub> sorbents. *J. Mater. Chem. A Mater.* **2016**, *4*, 14693–14702. [[CrossRef](#)]
120. Dou, X.; Hasa, I.; Saurel, D.; Vaalma, C.; Wu, L.; Buchholz, D.; Bresser, D.; Komaba, S.; Passerini, S. Hard carbons for sodium-ion batteries: Structure, analysis, sustainability, and electrochemistry. *Mater. Today* **2019**, *23*, 87–104. [[CrossRef](#)]
121. Klepel, O.; Hunger, B. Temperature-programmed desorption (TPD) of carbon dioxide on alkali-metal cation-exchanged faujasite type zeolites. *J. Therm. Anal. Calorim.* **2005**, *80*, 201–206. [[CrossRef](#)]
122. Jagiello, J.; Chojnacka, A.; Pourhosseini, S.E.M.; Wang, Z.; Beguin, F. A dual shape pore model to analyze the gas adsorption data of hierarchical micro-mesoporous carbons. *Carbon* **2021**, *178*, 113–124. [[CrossRef](#)]
123. Hotová, G.; Slovák, V.; Soares, O.S.G.P.; Figueiredo, J.L.; Pereira, M.F.R. Oxygen surface groups analysis of carbonaceous samples pyrolysed at low temperature. *Carbon* **2018**, *134*, 255–263. [[CrossRef](#)]
124. Wu, R.; Ye, Q.; Wu, K.; Wang, L.; Dai, H. Highly efficient CO<sub>2</sub> adsorption of corn kernel-derived porous carbon with abundant oxygen functional groups. *J. CO<sub>2</sub> Util.* **2021**, *51*, 101620. [[CrossRef](#)]
125. Xiao, J.; Wang, Y.; Zhang, T.C.; Ouyang, L.; Yuan, S. Phytic acid-induced self-assembled chitosan gel-derived N, P—Co-doped porous carbon for high-performance CO<sub>2</sub> capture and supercapacitor. *J. Power Sources* **2022**, *517*, 230727. [[CrossRef](#)]
126. Maklavany, D.M.; Rouzitalab, Z.; Amini, A.M.; Askarieh, M.; Silvestrelli, P.L.; Seif, A.; Orooji, Y.; Rashidi, A. One-step approach to Quaternary (B, N, P, S)-Doped hierarchical porous carbon derived from *Quercus Brantii* for highly selective and efficient CO<sub>2</sub> Capture: A combined experimental and extensive DFT study. *Chem. Eng. J.* **2023**, *453*, 139950. [[CrossRef](#)]
127. Ma, X.; Xu, W.; Su, R.; Shao, L.; Zeng, Z.; Li, L.; Wang, H. Insights into CO<sub>2</sub> capture in porous carbons from machine learning, experiments and molecular simulation. *Sep. Purif. Technol.* **2023**, *306*, 122521. [[CrossRef](#)]
128. Khodabakhshi, S.; Kiani, S.; Niu, Y.; White, A.O.; Suwaileh, W.; Palmer, R.E.; Barron, A.R.; Andreoli, E. Facile and environmentally friendly synthesis of ultramicroporous carbon spheres: A significant improvement in CVD method. *Carbon* **2021**, *171*, 426–436. [[CrossRef](#)]
129. Li, J.; Zhang, W.; Bao, A. Design of hierarchically structured porous boron/nitrogen codoped carbon materials with excellent performance for CO<sub>2</sub> capture. *Ind. Eng. Chem. Res.* **2021**, *60*, 2710–2718. [[CrossRef](#)]
130. Song, C.; Ye, W.; Liu, Y.; Huang, H.; Zhang, H.; Lin, H.; Lu, R.; Zhang, S. Facile preparation of porous carbon derived from industrial biomass waste as an efficient CO<sub>2</sub> adsorbent. *ACS Omega* **2020**, *5*, 28255–28263. [[CrossRef](#)]
131. Li, L.; Wang, X.F.; Zhong, J.J.; Qian, X.; Song, S.L.; Zhang, Y.G.; Li, D.H. Nitrogen-enriched porous polyacrylonitrile-based carbon fibers for CO<sub>2</sub> Capture. *Ind. Eng. Chem. Res.* **2018**, *57*, 11608–11616. [[CrossRef](#)]
132. Song, C.; Liu, M.; Ye, W.; Liu, Y.; Zhang, H.; Lu, R.; Zhang, S. Nitrogen-Containing Porous Carbon for Highly Selective and Efficient CO<sub>2</sub> Capture. *Energy Fuels* **2019**, *33*, 12601–12609. [[CrossRef](#)]
133. Xiong, L.; Wang, X.F.; Li, L.; Jin, L.; Zhang, Y.G.; Song, S.L.; Liu, R.P. Nitrogen-Enriched Porous Carbon Fiber as a CO<sub>2</sub> Adsorbent with Superior CO<sub>2</sub> Selectivity by Air Activation. *Energy Fuels* **2019**, *33*, 12558–12567. [[CrossRef](#)]
134. Mahurin, S.M.; Fulvio, F.; Hillesheim, C.; Nelson, K.M.; Veith, G.M.; Dai, S. Directed synthesis of nanoporous carbons from task-specific ionic liquid precursors for the adsorption of CO<sub>2</sub>. *ChemSusChem* **2014**, *7*, 3284–3289. [[CrossRef](#)] [[PubMed](#)]
135. Wang, X.F.; Xiong, L.; Zhong, J.J.; Jin, L.; Yan, J.L.; Mu, B.; Zhang, Y.G.; Song, S.L. Nitrogen-Containing Porous Carbon Fibers Prepared from Polyimide Fibers for CO<sub>2</sub> Capture. *Ind. Eng. Chem. Res.* **2020**, *59*, 18106–18114. [[CrossRef](#)]
136. Pevida, C.; Drage, T.C.; Snape, C.E. Silica-templated melamine-formaldehyde resin derived adsorbents for CO<sub>2</sub> capture. *Carbon* **2008**, *46*, 1464–1474. [[CrossRef](#)]
137. Li, D.; Chen, Y.; Zheng, M.; Zhao, H.; Zhao, Y.; Sun, Z. Hierarchically Structured Porous Nitrogen-Doped Carbon for Highly Selective CO<sub>2</sub> Capture. *ACS Sustain. Chem. Eng.* **2016**, *4*, 298–304. [[CrossRef](#)]
138. Estevez, L.; Barpaga, D.; Zheng, J.; Sabale, S.; Patel, R.L.; Zhang, J.G.; McGrail, B.P.; Motkuri, R.K. Hierarchically Porous Carbon Materials for CO<sub>2</sub> Capture: The Role of Pore Structure. *Ind. Eng. Chem. Res.* **2018**, *57*, 1262–1268. [[CrossRef](#)]
139. Hong, L.; Ju, S.; Liu, X.; Zhuang, Q.; Zhan, G.; Yu, X. Highly Selective CO<sub>2</sub> Uptake in Novel Fishnet-like Polybenzoxazine-Based Porous Carbon. *Energy Fuels* **2019**, *33*, 11454–11464. [[CrossRef](#)]
140. Wahab, M.A.; Na, J.; Masud, M.K.; Hossain, M.S.A.; Alothman, A.A.; Abdala, A. Nanoporous carbon nitride with a high content of inbuilt N site for the CO<sub>2</sub> capture. *J. Hazard Mater.* **2021**, *408*, 124843. [[CrossRef](#)]
141. Zeeshan, M.; Yalcin, K.; Oztuna, F.E.S.; Unal, U.; Keskin, S.; Uzun, A. A new class of porous materials for efficient CO<sub>2</sub> separation: Ionic liquid/graphene aerogel composites. *Carbon* **2021**, *171*, 79–87. [[CrossRef](#)]
142. Guo, Q.; Chen, C.; Li, Z.; Li, X.; Wang, H.; Feng, N.; Wan, H.; Guan, G. Controllable construction of N-enriched hierarchically porous carbon nanosheets with enhanced performance for CO<sub>2</sub> capture. *Chem. Eng. J.* **2019**, *371*, 414–423. [[CrossRef](#)]
143. Srinivas, G.; Krungleviciute, V.; Guo, Z.X.; Yildirim, T. Exceptional CO<sub>2</sub> capture in a hierarchically porous carbon with simultaneous high surface area and pore volume. *Energy Environ. Sci.* **2014**, *7*, 335–342. [[CrossRef](#)]
144. Kumbhar, D.; Palliyarayil, A.; Reghu, D.; Shrunagar, D.; Umapathy, S.; Sil, S. Rapid discrimination of porous bio-carbon derived from nitrogen rich biomass using Raman spectroscopy and artificial intelligence methods. *Carbon* **2021**, *178*, 792–802. [[CrossRef](#)]

145. Ma, C.; Bai, J.; Hu, X.; Jiang, Z.; Wang, L. Nitrogen-doped porous carbons from polyacrylonitrile fiber as effective CO<sub>2</sub> adsorbents. *J. Environ. Sci.* **2023**, *125*, 533–543. [[CrossRef](#)] [[PubMed](#)]
146. Alloush, A.M.; Abdulghani, H.; Amasha, H.A.; Saleh, T.A.; Al Hamouz, O.C.S. Microwave-assisted synthesis of novel porous organic polymers for effective selective capture of CO<sub>2</sub>. *J. Ind. Eng. Chem.* **2022**, *113*, 215–225. [[CrossRef](#)]
147. Gou, J.; Liu, C.; Lin, J.; Yu, C.; Fang, Y.; Liu, Z.; Guo, Z.; Tang, C.; Huang, Y. Densification and pelletization of porous boron nitride fibers for effective CO<sub>2</sub> adsorption. *Ceram. Int.* **2022**, *48*, 11636–11643. [[CrossRef](#)]
148. Dhoke, C.; Zaabout, A.; Cloete, S.; Amini, S. Review on reactor configurations for adsorption-based CO<sub>2</sub> capture. *Ind. Eng. Chem. Res.* **2021**, *60*, 3779–3798. [[CrossRef](#)]
149. Zhang, R.; Li, Z.; Zeng, L.; Wang, F. Pressure drop in honeycomb adsorption filters filled with granular activated carbon. *Powder Technol.* **2021**, *393*, 550–558. [[CrossRef](#)]
150. Rezaei, F.; Grahn, M. Thermal management of structured adsorbents in CO<sub>2</sub> capture processes. *Ind. Eng. Chem. Res.* **2012**, *51*, 4025–4034. [[CrossRef](#)]
151. Rezaei, F.; Webley, P. Structured adsorbents in gas separation processes. *Sep. Purif. Technol.* **2010**, *70*, 243–256. [[CrossRef](#)]
152. Rezaei, F.; Webley, P. Optimum structured adsorbents for gas separation processes. *Chem. Eng. Sci.* **2009**, *64*, 5182–5191. [[CrossRef](#)]
153. Akhtar, F.; Andersson, L.; Ogunwumi, S.; Hedin, N.; Bergström, L. Structuring adsorbents and catalysts by processing of porous powders. *J. Eur. Ceram. Soc.* **2014**, *34*, 1643–1666. [[CrossRef](#)]
154. Borchardt, L.; Michels, N.L.; Nowak, T.; Mitchell, S.; Pérez-Ramírez, J. Structuring zeolite bodies for enhanced heat-transfer properties. *Microporous Mesoporous Mater.* **2015**, *208*, 196–202. [[CrossRef](#)]
155. Tang, S.H.; Zaini, M.A.A. Development of activated carbon pellets using a facile low-cost binder for effective malachite green dye removal. *J. Clean. Prod.* **2020**, *253*, 119970. [[CrossRef](#)]
156. Cousin-Saint-Remi, J.; Van der Perre, S.; Segato, T.; Delplancke, M.P.; Goderis, S.; Terryn, H.; Baron, G.; Denayer, J. Highly Robust MOF Polymeric Beads with a Controllable Size for Molecular Separations. *ACS Appl Mater Interfaces* **2019**, *11*, 13694–13703. [[CrossRef](#)]
157. Valizadeh, B.; Nguyen, T.N.; Smit, B.; Stylianou, K.C. Porous Metal–Organic Framework@Polymer Beads for Iodine Capture and Recovery Using a Gas-Sparged Column. *Adv. Funct. Mater.* **2018**, *28*, 1801596. [[CrossRef](#)]
158. de Almeida Moreira, B.R.; Cruz, V.H.; Pérez, J.F.; da Silva Viana, R. Production of pellets for combustion and physisorption of CO<sub>2</sub> from hydrothermal carbonization of food waste—Part I: High-performance solid biofuels. *J. Clean. Prod.* **2021**, *319*, 128695. [[CrossRef](#)]
159. Kim, Y.J.S. Adsorption of Carbon Dioxide using Pelletized AC with Amine impregnation. *J. Korean Oil Chem. Soc.* **2013**, *30*, 88–89. [[CrossRef](#)]
160. Manohara, G.V.; Maroto-Valer, M.M.; Garcia, S. Binder free novel synthesis of structured hybrid mixed metal oxides (MMOs) for high temperature CO<sub>2</sub> capture. *Chem. Eng. J.* **2021**, *415*, 128881. [[CrossRef](#)]

**Disclaimer/Publisher’s Note:** The statements, opinions and data contained in all publications are solely those of the individual author(s) and contributor(s) and not of MDPI and/or the editor(s). MDPI and/or the editor(s) disclaim responsibility for any injury to people or property resulting from any ideas, methods, instructions or products referred to in the content.